

Membership Inference Attacks from Causal Principles

Mathieu Even¹ Clément Berenfeld¹ Linus Bleistein² Tudor Cebere¹ Julie Josse¹ Aurélien Bellet¹

Abstract

Membership Inference Attacks (MIAs) are widely used to quantify training data memorization and assess privacy risks. Standard evaluation requires repeated retraining, which is computationally costly for large models. One-run methods (single training with randomized data inclusion) and zero-run methods (post hoc evaluation) are often used instead, though their statistical validity remains unclear. To address this gap, we frame MIA evaluation as a causal inference problem, defining *memorization as the causal effect of including a data point* in the training set. This novel formulation reveals and formalizes key sources of bias in existing protocols: one-run methods suffer from interference between jointly included points, while zero-run evaluations popular for LLMs are confounded by non-random membership assignment. We derive causal analogues of standard MIA metrics and propose practical estimators for multi-run, one-run, and zero-run regimes with non-asymptotic consistency guarantees. Experiments on real-world data show that our approach enables reliable memorization measurement even when retraining is impractical and under distribution shift, providing a principled foundation for privacy evaluation in modern AI systems.

1. Introduction

The rapid deployment of large-scale machine learning models has intensified concerns regarding data privacy and intellectual property. Prior work has shown that these models are susceptible to various privacy attacks capable of inferring sensitive information about individual training data points (Shokri et al., 2017; Carlini et al., 2019; 2021; Nasr et al., 2023a; Barbero et al., 2025; Hayes et al., 2025). Consequently, data owners and regulators increasingly question

¹PreMeDICaL team, Inria, Idesp, Inserm, Université de Montpellier ²School of Computer and Communication Science (EPFL) and School of Life Sciences (EPFL). Correspondence to: Aurélien Bellet <aurelien.bellet@inria.fr>.

whether unauthorized information has been added to training sets, potentially exposing personal or copyrighted content. Recent guidance from data protection authorities emphasizes the use of attack-based evaluations to assess privacy leakage and to determine whether a trained model may itself constitute personal data under existing regulatory frameworks (European Data Protection Board, 2024), while recent high-profile legal challenges concerning data provenance and usage have raised similar questions regarding whether specific data was used in model training (New York Times v. OpenAI, 2023; Concord Music Group v. Anthropic, 2023).

In this context, *Membership Inference Attacks* (MIAs) offer a compelling conceptual and practical tool, as they probe the minimal form of information a model can retain about a data point: whether it was part of the training set (Carlini et al., 2022). MIAs provide a principled measure of memorization and unintended privacy leakage, revealing when a model’s internal representations encode training-specific artifacts that distinguish members from non-members, even when direct data leakage is rare or difficult to observe. MIAs also play a key role in auditing differential privacy (Jagielski et al., 2020; Nasr et al., 2023b) and enabling other privacy attacks, including data reconstruction (Carlini et al., 2021; 2019; Nasr et al., 2023a; Barbero et al., 2025) and dataset inference (Maini et al., 2021; 2024).

The standard framework for evaluating MIAs, the *multi-run* regime, involves retraining models hundreds or thousands of times with and without a given point (Shokri et al., 2017; Yeom et al., 2018; Carlini et al., 2022; Zarifzadeh et al., 2024). While statistically rigorous, this approach is computationally prohibitive for modern large-scale models, prompting a shift toward more efficient alternatives. In *one-run* approaches, a single model is trained on a randomized subset of data (Steinke et al., 2023; Mahloujifar et al., 2024; Liu et al., 2025), whereas *zero-run* methods evaluate a deployed model post hoc (Ye et al., 2022; Shi et al., 2023; Bertran et al., 2023; Meeus et al., 2024a). This latter scenario is particularly relevant when an external evaluator cannot directly intervene in model training, which requires provider cooperation and trust, and cannot independently retrain the model due to withheld information about the training data or algorithm, as typically the case when using MIAs to assess the privacy risks of LLMs deployed by dominant tech companies.

However, when moving from controlled retraining to more practical settings, the statistical validity of MIA evaluation becomes unclear. In particular, recent work shows that zero-run MIAs on LLMs suffer from *systematic bias* caused by distribution shift in the non-member data used for evaluation (Duan et al., 2024; Zhang et al., 2024; Meeus et al., 2024b). For example, in typical evaluations of LLMs with a fixed training cutoff date, *members* are documents published before the cutoff—e.g., arXiv papers or Wikipedia articles that were almost certainly included in training—while *non-members* are documents published afterward. These sets often differ in topic, style, and temporal context, so MIA success may reflect such distributional differences rather than true memorization, overestimating the model’s memorization (Meeus et al., 2024b).

Contributions. In this work, we reframe the evaluation of MIAs as a causal inference problem, *defining memorization as the causal effect of including a data point in the training set*. This shift from a predictive to a causal perspective allows us to explicitly identify the assumptions required to interpret MIA performance as genuine memorization rather than an artifact of confounding factors, and to design robust estimators that eliminate the systematic biases of existing approaches. Specifically, our contributions are as follows:

1. **Causal formalization of MIAs:** We introduce a causal formulation of MIAs grounded in the potential outcomes framework (Imbens & Rubin, 2015; Wager, 2024). Drawing on classical causal estimands, we define causal counterparts to traditional MIA metrics. Our framework isolates the effect of a training point on the model’s output, removing non-causal signals that can distort memorization assessments, and shifting the focus of MIA evaluation from correlation to causation.
2. **A causal taxonomy:** We analyze multi-run, one-run, and zero-run MIA evaluations from a causal lens, formalizing their distinct sources of error. These include *interference* (Hudgens & Halloran, 2008) between jointly inserted points in one-run settings, and *confounding* (Rosenbaum & Rubin, 1983) arising from non-random assignments in zero-run scenarios.
3. **Principled estimators:** We propose practical estimators for causal MIA metrics that explicitly correct the distribution shift bias discussed above, and provide non-asymptotic consistency guarantees showing these quantities are identifiable in practice. As a byproduct, we derive a new approach with consistency results for causal effects under random interference, a challenging setting (Cinelli et al., 2025), by leveraging learning-theoretic tools such as algorithmic stability (Bousquet & Elisseeff, 2002) in a novel way.
4. **Empirical validation:** Through experiments on synthetic data and CIFAR-10, we demonstrate that our causal estimators provide practical and reliable

solutions to the challenges of MIA evaluation.

2. Background

Since MIAs and causal inference are generally studied by different communities, we review the necessary background from both areas, adopting consistent notations.

2.1. Membership Inference Attacks (MIAs)

An MIA aims to determine whether a specific record $x \in \mathcal{X}$ was included in a model’s training set. A training algorithm \mathcal{A} is a (potentially randomized) function that maps a dataset $\mathcal{D} \subset \mathcal{X}$ to model parameters $\theta = \mathcal{A}(\mathcal{D})$ in a parameter space $\Theta \subset \mathbb{R}^D$. MIAs use a scoring function $s_{\text{MIA}}(x, \theta) \in \mathbb{R}$ (e.g., loss or log-likelihood of θ on x) to compute a *membership confidence score*, which is typically thresholded to predict membership. In this work, our focus is not on designing MIAs (i.e., constructing a suitable s_{MIA}), but on the validity of their evaluation across the regimes shown in Figure 1, which differ in how they collect the evidence $(X_i, A_i, Y_i)_{i \in [n]}$, where $X_i \in \mathcal{X}$ is a data point, $A_i \in \{0, 1\}$ is its membership in the training set, and Y_i is its MIA score. Evaluating MIAs requires specifying the distribution over which memorization is measured; throughout the paper, we denote this target distribution by \mathcal{P}_T .

Multi-run (Algorithm 1). Each sample (X_i, A_i, Y_i) is generated from an independently trained model θ_i , where $X_i \sim \mathcal{P}_T$ and the membership variable A_i is randomized.

One-run (Algorithm 2). Introduced by Steinke et al. (2023), this regime trains a single model with n points drawn from \mathcal{P}_T randomly included in the training set $\mathcal{D}_{\text{train}}$.

Zero-run (Algorithm 3). As in recent studies on LLMs (Shi et al., 2023; Mattern et al., 2023; Meeus et al., 2024a), this regime evaluates MIAs post-hoc on a fixed model, without retraining. The training set $\mathcal{D}_{\text{train}}$ is fixed and unknown to the evaluator. Evaluation uses proxy datasets: $\mathcal{D}_T \subset \mathcal{D}_{\text{train}}$ (known members, e.g., pre-2023 Wikipedia) and $\mathcal{D}_0 \subset \mathcal{X} \setminus \mathcal{D}_{\text{train}}$ (known non-members, e.g., post-release articles).

Evaluation metrics. The evidence $(X_i, A_i, Y_i)_{i \in [n]}$ is used to compute standard MIA performance metrics, measuring memorization by how well the scores Y_i separate members ($A_i = 1$) from non-members ($A_i = 0$): **(i) Membership advantage:** $\mathbb{E}[Y_i | A_i = 1] - \mathbb{E}[Y_i | A_i = 0]$; **(ii) AUC:** $\mathbb{P}(Y_i > Y_j | A_i = 1, A_j = 0)$; **(iii) TPR at fixed FPR:** $\mathbb{P}(Y_i \geq t_\alpha | A_i = 1)$ with t_α the $(1 - \alpha)$ -quantile of $Y_i | A_i = 0$.

2.2. Causal Inference

In causal inference (Hernán & Robins, 2010; Rubin, 1974; Wager, 2024), observations are tuples (X_i, A_i, Y_i) , where X_i denotes covariates, $A_i \in \{0, 1\}$ is a treatment indicator,

Algorithm 1 Multi-run	Algorithm 2 One-run	Algorithm 3 Zero-run
<pre> 1: Input: algorithm \mathcal{A}, dataset \mathcal{D}, target distribution \mathcal{P}_T, number of samples n 2: for $i \in [n]$ do 3: Sample $X_i \sim \mathcal{P}_T$ 4: $A_i \sim \text{Bernoulli}(1/2)$ 5: $\mathcal{D}_{\text{train},i} \leftarrow \begin{cases} \mathcal{D} \cup \{X_i\} & \text{if } A_i = 1, \\ \mathcal{D} & \text{otherwise.} \end{cases}$ 6: $\theta_i \leftarrow \mathcal{A}(\mathcal{D}_{\text{train},i})$ 7: $Y_i \leftarrow s_{\text{MIA}}(X_i, \theta_i)$ 8: end for 9: Output: $(X_i, A_i, Y_i)_{i \in [n]}$ </pre>	<pre> 1: Input: algorithm \mathcal{A}, dataset \mathcal{D}, target distribution \mathcal{P}_T, number of samples n 2: for $i \in [n]$ do 3: Sample $X_i \sim \mathcal{P}_T$ 4: $A_i \sim \text{Bernoulli}(1/2)$ 5: end for 6: $\mathcal{D}_{\text{train}} \leftarrow \mathcal{D} \cup \{X_i : A_i = 1\}$ 7: $\theta \leftarrow \mathcal{A}(\mathcal{D}_{\text{train}})$ 8: for $i \in [n]$ do 9: $Y_i \leftarrow s_{\text{MIA}}(X_i, \theta)$ 10: end for 11: Output: $(X_i, A_i, Y_i)_{i \in [n]}$ </pre>	<pre> 1: Input: trained model $\theta \leftarrow \mathcal{A}(\mathcal{D}_{\text{train}})$, datasets $\mathcal{D}_T \subset \mathcal{D}_{\text{train}}$ (of underlying distribution \mathcal{P}_T) and $\mathcal{D}_0 \subset \mathcal{X} \setminus \mathcal{D}_{\text{train}}$ 2: $(X_i)_{i \in [n]} \leftarrow \mathcal{D}_T \cup \mathcal{D}_0$ 3: for $i \in [n]$ do 4: $A_i \leftarrow \mathbb{1}_{\{X_i \in \mathcal{D}_T\}}$ 5: $Y_i \leftarrow s_{\text{MIA}}(X_i, \theta)$ 6: end for 7: Output: $(X_i, A_i, Y_i)_{i \in [n]}$ </pre>

Figure 1. MIA evaluation scenarios studied in this work, with the MIA abstracted by its score function s_{MIA} . Green highlights the key steps of the multi-run setting; red indicates the successive modifications introduced when moving to the one-run and zero-run settings.

and Y_i is here a real-valued outcome. Under the potential outcomes framework (Splawa-Neyman et al., 1990), each unit has two counterfactual outcomes $Y_i(0)$ and $Y_i(1)$, but only $Y_i = Y_i(A_i)$ is observed. Individual treatment effects $Y_i(1) - Y_i(0)$ are thus not identifiable, meaning they cannot be uniquely determined from the distribution of the observed data. Causal inference instead focuses on population-level quantities such as the average treatment effect (ATE) $\mathbb{E}[Y_i(1) - Y_i(0)]$, which are identifiable under standard assumptions.

Assumption 2.1 (Standard causal assumptions). $\forall i \in [n]$,

1. (SUTVA) $Y_i = Y_i(A_i)$;
2. The assignment mechanism satisfies either:
 - (a) (Randomized) $A_i \perp\!\!\!\perp (Y_i(0), Y_i(1))$;
 - (b) (Unconfoundedness) $A_i \perp\!\!\!\perp (Y_i(0), Y_i(1)) | X_i$;
3. (Overlap) $0 < \mathbb{P}(A_i = 1 | X_i) < 1$ almost surely.

SUTVA and overlap imply a unit’s outcome does not depend on other units’ assignments, and that each unit has a nonzero probability of receiving either treatment. The assumption on the assignment mechanism depends on the setting.

RCT vs observational study. In randomized control trials (RCTs), treatment is assigned randomly to each unit, so the *Randomized* assumption holds. In observational studies, treatment may correlate with covariates that also affect outcomes, violating this assumption. *Unconfoundedness* addresses this by requiring that, conditional on observed covariates, treatment assignment is as good as random.

Causal inference with interference. When the SUTVA assumption is violated, *interference* occurs: a unit’s outcome may depend on other units’ treatment assignments, for instance through shared resources, competition effects, or herd immunity in vaccine trials (Sobel, 2006). Causal inference with interference thus requires additional formalism (Hudgens & Halloran, 2008). Specifically, interference is modeled by generalized potential outcomes

$Y_i(\bar{a})$ indexed by the full assignment vector $\bar{a} \in \{0, 1\}^n$, with observed outcome $Y_i = Y_i(\bar{A})$ for $\bar{A} = (A_j)_{j \in [n]}$. We define the marginal potential outcome as:

$$Y_i(a) = Y_i(A_1, \dots, A_{i-1}, a, A_{i+1}, \dots, A_n). \quad (1)$$

In the absence of interference, $Y_i(\bar{a}) = Y_i(a_i)$, recovering the standard setting. Standard causal assumptions under interference (Ogburn et al., 2024) that generalize Assumption 2.1 are detailed in Appendix A.1.

3. MIA Evaluation Under a Causal Lens

Our first and main contribution is to frame membership inference as a causal question: *what is the effect of including a given data point in the training set on the model?* In this formulation, the *treatment* A_i is the inclusion of a data point X_i in the training set, and the *outcome* Y_i is the membership confidence score (which depends on both the model and the data point X_i). Potential outcomes $Y_i(1)$ and $Y_i(0)$ correspond to the model’s output on X_i under two counterfactual worlds: one in which X_i was used for training and one in which it was not. Since only one of these worlds is observed, individual effects are unidentifiable, but population-level causal effects can be estimated. Casting membership inference in this causal framework clarifies what is being measured and enables principled control of interference and confounding that would otherwise bias the evaluation.

3.1. Causal Interpretation of Evaluation Regimes

We now explicitly map the three scenarios corresponding to Algorithms 1 to 3 to standard causal inference settings, with their corresponding causal graphs shown in Figure 2.

Multi-run \leftrightarrow RCT. The treatment is randomized and (X_i, A_i, Y_i) are i.i.d., corresponding to a standard RCT setting in causal inference where Assumption 2.1 with randomized assignments holds by design.

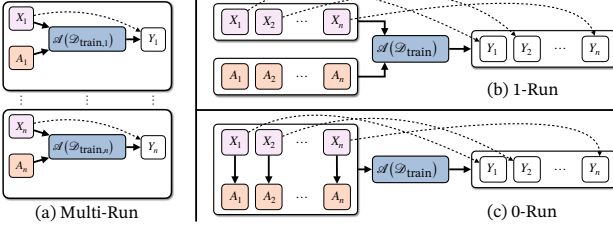


Figure 2. Causal graphs for the three different evaluation paradigms for MIAs. (a) In the multi-run setting, inclusion of a point is randomized, and for every point, a separate model is trained. (b) In the 1-run setting, inclusion of every point is randomized, but only one model is trained. (c) In the 0-run setting, data inclusion is not randomized, and the model is only trained once.

One-run \leftrightarrow RCT with interference. While the randomized assignment property is preserved, the one-run setting trades computational efficiency (training a single model instead of n) for the presence of *interference* between units. Indeed, the assignment A_j of point $j \in [n]$ can affect Y_i for $i \neq j$, since including or excluding X_j changes the learned model used to compute all outcomes. The one-run regime thus corresponds to an RCT with interference. In the causal graph shown in Figure 2b), interference arises through the shared mediator $A(\mathcal{D}_{\text{train}})$. Without this mediator, the graph would contain direct edges $A_i \rightarrow Y_j$ for all $i, j \in [n]$, corresponding to a complete interference graph. While causal quantities are identifiable under standard assumptions (Assumption A.1) that here hold by design, assumptions will be required to ensure the consistency of our estimators. Crucially, our assumptions will be on the learning algorithm itself, representing a novel approach to ensuring estimator consistency under complete interference.

Zero-run \leftrightarrow observational study with interference. This setting inherits interference from the one-run scenario and adds *confounding*. As shown by the edge from X_i to A_i in Figure 2c), membership is not assigned independently of the data points due to the distribution shift between members and non-members. This confounding factor, which is at the heart of misleading conclusions observed in memorization studies for LLMs (Meeus et al., 2024b), turns the problem into an *observational study*. Framing the problem causally makes this shift explicit and will enable principled debiasing of evaluation metrics via confounder adjustment.

3.2. Causal MIA Evaluation Metrics

When members ($A = 1$) and non-members ($A = 0$) follow different distributions, the evaluation metrics defined in Section 2.1 may conflate true memorization effects—i.e., differences in Y_i versus Y_j for $A_i \neq A_j$ even when $X_i \approx X_j$ —with distribution shift effects, where differences in Y arise simply because X_i and X_j differ. To address this, we introduce causal metrics that enable meaningful MIA evaluation

Table 1. Classical MIA metrics and their causal counterparts.

Classical metrics	Causal metrics
Membership Advantage $\mathbb{E}[Y_i A_i=1] - \mathbb{E}[Y_i A_i=0]$	Average Treatment Effect $\mathbb{E}_{\mathcal{P}_T}[Y_i(1) - Y_i(0)]$
$\text{TPR}(t) = \mathbb{P}(Y_i > t A_i=1)$ $\text{FPR}(t) = \mathbb{P}(Y_i > t A_i=0)$	$\tau_{\text{TPR}}(t) = \mathbb{P}_{\mathcal{P}_T}(Y_i(1) > t)$ $\tau_{\text{FPR}}(t) = \mathbb{P}_{\mathcal{P}_T}(Y_i(0) > t)$
AUC Area under $\{\text{FPR}(t), \text{TPR}(t)\}$	Causal AUC Area under $\{\tau_{\text{FPR}}(t), \tau_{\text{TPR}}(t)\}$
TPR at fixed FPR α $\mathbb{P}(Y_i \geq t_\alpha A_i=1)$ $t_\alpha: 1-\alpha$ quantile of $Y_i A_i=0$	Causal TPR at fixed FPR α $\mathbb{P}_{\mathcal{P}_T}(Y_i(1) \geq q_\alpha)$ $q_\alpha: 1-\alpha$ quantile of $Y_i(0) X_i \sim \mathcal{P}_T$

under both interference and distribution shift. Table 1 summarizes these metrics alongside their corresponding classical counterparts. Below, $\mathbb{E}_{\mathcal{P}_T}$ and $\mathbb{P}_{\mathcal{P}_T}$ denote expectations and probabilities over $X_i \sim \mathcal{P}_T$, where \mathcal{P}_T is the target distribution. Under interference, all causal quantities implicitly depend on the dataset size n , as can be seen from (1).

Causal membership advantage (ATE). The Average Treatment Effect (ATE) is given by

$$\tau_{\text{ATE}} = \mathbb{E}_{\mathcal{P}_T}[Y_i(1) - Y_i(0)]. \quad (2)$$

When membership confidence scores can be interpreted as estimated membership probabilities, τ_{ATE} admits a direct interpretation as a *causal membership advantage*.

Causal AUC. For a threshold $t \in \mathbb{R}$, we define causal versions of TPR and FPR as $\tau_{\text{TPR}}(t) = \mathbb{P}_{\mathcal{P}_T}(Y_i(1) \geq t)$ and $\tau_{\text{FPR}}(t) = \mathbb{P}_{\mathcal{P}_T}(Y_i(0) \geq t)$. The causal ROC curve is then defined as $\{(\tau_{\text{FPR}}(t), \tau_{\text{TPR}}(t))\}_{t \in \mathbb{R}}$, while the causal AUC is defined as the area under the causal ROC curve.

Causal TPR at fixed FPR. We define the causal TPR at fixed FPR α as $\tau_{\text{TPR}@\text{FPR}}(\alpha) = \mathbb{P}_{\mathcal{P}_T}(Y_i(1) \geq q_\alpha)$, with q_α the $1 - \alpha$ quantile of $Y_i(0)|X_i \sim \mathcal{P}_T$.

4. MIA Evaluation in the Multi-Run Setting

In the multi-run setting, identification follows from Assumption 2.1, which is satisfied by design.

Proposition 4.1. Assume that $(X_i, A_i, Y_i)_{i \in [n]}$ are obtained using Algorithm 1. Then, the causal evaluation metrics (right column of Table 1) are identifiable and are equal to the classical evaluation metrics (left column of Table 1).

These properties then enable estimation of the causal evaluation metrics. Due to space constraints, we focus here on estimators of the ATE (the causal *membership advantage*); estimators and consistency results for the other causal metrics are provided in Appendix C. Let

$$\hat{\tau}_{\text{ATE}} = \frac{1}{n_1} \sum_{i: A_i=1} Y_i - \frac{1}{n_0} \sum_{i: A_i=0} Y_i, \quad (3)$$

for $n_1 = \#\{i : A_i = 1\}$ and $n_0 = \#\{i : A_i = 0\}$.

Proposition 4.2. Assume that $(X_i, A_i, Y_i)_{i \in [n]}$ are obtained using Algorithm 1. Then, $\hat{\tau}_{ATE}$ is a consistent estimator of τ_{ATE} . Furthermore, if outcomes Y_i are in $[0, 1]$ almost surely,¹ with probability $1 - 4e^{-t}$ we have:

$$|\hat{\tau}_{ATE} - \tau_{ATE}| \leq \sqrt{\frac{2t}{n_1}} + \sqrt{\frac{2t}{n_0}}.$$

5. Handling Interference in One-Run

We now consider the one-run setting, in which SUTVA in Assumption 2.1 is violated due to *interference*, so identification is no longer straightforward. We remind that we work with generalized counterfactuals: for $\bar{a} \in \{0, 1\}^n$, $Y_i(\bar{a})$ is the outcome of unit $i \in [n]$ we would have observed had treatment assignments been $A_j = a_j$ for all $j \in [n]$, thereby explicitly modeling interference between data points. A generalization of Assumption 2.1 to settings with interference is provided in Appendix A.1 and holds by design, allowing us to generalize Proposition 4.1 to the one-run setting.

Proposition 5.1. Assume that $(X_i, A_i, Y_i)_{i \in [n]}$ are obtained using Algorithm 2. Then the causal evaluation metrics (right column of Table 1) are identifiable and equal to the classic evaluation metrics (left column of Table 1).

We consider the same estimators as in the multi-run setting, such as $\hat{\tau}_{ATE}$ defined in Equation (3) for the ATE. Consistency, however, is no longer guaranteed, since interference induces dependence between samples. As aptly noted by Cinelli et al. (2025, Section 3.2), “all no-interference applications are alike; each SUTVA violation violates SUTVA in its own way”, underscoring the absence of a one-size-fits-all solution for handling interference. In our setting, as illustrated in Figure 2b, interference arises because a single model is trained jointly on all members, inducing a complete interference graph over data points. We thus propose to impose assumptions directly on the training algorithm \mathcal{A} , since the interference structure is intrinsic and unavoidable.

To this end, we leverage learning-theoretic notions that formalize limited sensitivity of a model’s behavior to any single training point. The first, *error stability*, is milder than classical uniform stability (satisfied by regularized ERM (Bousquet & Elisseeff, 2002) and SGD on convex or smooth nonconvex objectives with Lipschitz losses (Hardt et al., 2016)) and controls changes in average test loss. Error stability controls the change in average test loss. The second, *uniform training stability*, bounds changes in the loss at any training point.

Definition 5.2 (Error stability; Bousquet & Elisseeff, 2002). A learning algorithm \mathcal{A} is α -error stable with respect to a loss \mathcal{L} if for all datasets $\mathcal{D} = \{x_1, \dots, x_n\}$, all $i \in [n]$ and \mathcal{D}' such that $\mathcal{D}' = \{x'_1, \dots, x'_n\}$ with $x_j = x'_j$ if $j \neq i$, for

¹Our results readily extend to outcomes in a bounded space of diameter B , via a rescaling of the results by B .

$X \sim \mathcal{P}_T$ independent of the rest, we have:

$$|\mathbb{E}_{\mathcal{A}}[\mathbb{E}_X[\mathcal{L}(\mathcal{A}(\mathcal{D}), X)]] - \mathbb{E}_{\mathcal{A}}[\mathbb{E}_X[\mathcal{L}(\mathcal{A}(\mathcal{D}'), X)]]| \leq \alpha,$$

where $\mathcal{L}(\theta, x)$ denotes the loss of model θ at $x \in \mathcal{X}$.

Definition 5.3 (β -uniform training stability). A learning algorithm \mathcal{A} is β -interpolating with respect to a loss \mathcal{L} if for all datasets $\mathcal{D} = \{x_1, \dots, x_n\}$, all $i \in [n]$ and \mathcal{D}' such that $\mathcal{D}' = \{x'_1, \dots, x'_n\}$ with $x_j = x'_j$ if $j \neq i$, for any $k \in [n] \setminus \{i\}$, we have:

$$|\mathcal{L}(\mathcal{A}(\mathcal{D}), x_k) - \mathcal{L}(\mathcal{A}(\mathcal{D}'), x_k)| \leq \beta.$$

Definition 5.3 is trivially satisfied by uniformly stable algorithms, with β equal to the uniform stability parameter. Moreover, interpolating models, whose loss is minimal on all training points, satisfy β -uniform training stability with $\beta = 0$, while models close to the interpolation regime (i.e., with small training loss) satisfy it for a small constant β .

Theorem 5.4. Assume that $(X_i, A_i, Y_i)_{i \in [n]}$ are obtained using Algorithm 2, with $Y_i = \mathcal{L}(\theta, X_i)$ corresponding to the standard loss-based attack. Assume that \mathcal{A} is α -error stable (Definition 5.2), β -uniform training stable (Definition 5.3), and that outcomes Y_i are in $[0, 1]$ almost surely. Then, with probability $1 - Ce^{-t}$ for some numerical constant $C > 0$:

$$|\hat{\tau}_{ATE} - \tau_{ATE}| = \mathcal{O}\left(\sqrt{\frac{t}{n}} + \sqrt{nt\alpha^2} + \sqrt{nt\beta^2}\right).$$

In the perfect interpolation regime ($\beta = 0$), the first term $\sqrt{t/n}$ is expected and tends to 0. For consistency, we thus need the second term $\sqrt{nt\alpha^2}$ to also be negligible, which is the case as long as the stability parameter $\alpha = o(1/\sqrt{n})$. For regularized convex or strongly convex problems, this will always hold since then α is of order $1/N$ where N is the total number of training points in \mathcal{D}_{train} , leading to $\sqrt{nt\alpha^2} = \mathcal{O}(1/\sqrt{N})$ where $N \geq n$. In most applications, n will be negligible in front of N , so the second term becomes negligible in front of the first. For nonconvex problems, error stability no longer holds in general, but for SGD training with smooth, Lipschitz losses and early-stopping, error stability holds with α of order $N^{-1+o(1)}$ (Hardt et al., 2016). The term $\alpha\sqrt{n}$ will thus be of order $1/\sqrt{N}$ if $n = \mathcal{O}(N^{1-o(1)})$. In the general case, β is also required to be small enough. This is the case for large overparametrized and near-interpolating networks, or for uniformly stable algorithms. We also show in Appendix B that under an underparametrized regime (i.e., $\frac{D}{n} \rightarrow 0$), no MIA attack based on the loss can be successful ($\tau_{ATE} \approx 0$).

Remark 5.5 (Extension to other MIAs). Consistency results in this section are specific to the loss-based MIA, as this allows us to invoke standard learning-theoretic assumptions (Definitions 5.2 and 5.3). Extending Theorem 5.4 to other MIAs would require assuming stability of the confidence score function s_{MIA} , rather than stability of the loss itself.

6. Adjusting for Confounders in Zero-Run

In the zero-run regime, the presence of confounders introduces an additional challenge for identifying and estimating causal evaluation metrics, due to the distributional shift between member data (\mathcal{D}_T) and non-member data (\mathcal{D}_0). Indeed, the problem departs from a RCT and becomes an observational study, since $\mathcal{P}_{X_i|A_i=1} \neq \mathcal{P}_{X_i|A_i=0}$. As is standard in causal inference, observational studies cannot be conducted without assumptions: the identifiability of causal estimands (such as τ_{ATE}) depends on them. We thus assume that any member in \mathcal{D}_T would have had a non-zero probability of appearing in \mathcal{D}_0 (non-member data).

Assumption 6.1 (Domain overlap). \mathcal{D}_T and \mathcal{D}_0 consist of independent samples from distributions \mathcal{P}_T and \mathcal{P}_0 , respectively, with $\frac{d\mathcal{P}_T}{d\mathcal{P}_0}(x) < \infty$ for all $x \in \text{Supp}(\mathcal{P}_T)$.

Under this assumption, *overlap* holds (Assumption 2.1) together with identifiability, as we show next for τ_{ATE} (see Appendix C for a generalization to the other causal metrics). Note that under Assumption 6.1 we have $\mathcal{P}_T = \mathcal{P}_{X_i|A_i=1}$ and $\mathcal{P}_0 = \mathcal{P}_{X_i|A_i=0}$.

Proposition 6.2. *Under Assumption 6.1, if $(X_i, A_i, Y_i)_{i \in [n]}$ are obtained according to Algorithm 3, the causal evaluation metrics are identifiable. Furthermore, let*

$$\pi(x) = \mathbb{P}(A_i = 1 | X_i = x), \quad \forall x \in \mathcal{X}. \quad (4)$$

Then, we have:

$$\tau_{ATE} = \frac{\mathbb{E}[A_i Y_i]}{\mathbb{P}(A_i=1)} - \frac{\mathbb{E}\left[\frac{\pi(X_i)(1-A_i)}{1-\pi(X_i)} Y_i\right]}{\mathbb{P}(A_i=0)}. \quad (5)$$

Equation (5) highlights the fact that with confounders, the right and left column of Table 1 are no longer equal. Using estimators of traditional evaluation metrics (left column) thus leads to biases when evaluating MIA performance. Indeed, estimators such as $\hat{\tau}_{ATE}$ in (3) would estimate $\mathbb{E}[Y_i | A_i = 1] - \mathbb{E}[Y_i | A_i = 0]$ instead of τ_{ATE} , which is different since $\mathcal{P}_{Y_i|A_i=0} \neq \mathcal{P}_{Y_i(0)|A_i=1}$ due to the fact that $\mathcal{P}_0 = \mathcal{P}_{X_i|A_i=0} \neq \mathcal{P}_{X_i|A_i=1} = \mathcal{P}_T$.

Equation (5) in Proposition 4.1 naturally motivates an *inverse probability weighting* (IPW) estimator:

$$\hat{\tau}_{ATE}^{(IPW)} = \frac{1}{n_1} \sum_{A_i=1} Y_i - \frac{1}{n_0} \sum_{A_i=0} \frac{\hat{\pi}(X_i)}{1-\hat{\pi}(X_i)} Y_i, \quad (6)$$

where $\hat{\pi}$ is an estimate of the *propensity score* π defined in (4). The estimator (6) belongs to the classical family of IPW debiasing methods widely used in causal inference with observational data (Rosenbaum & Rubin, 1983).²

The propensity score estimator $\hat{\pi}$ can be obtained by training any probabilistic binary classifier $\mathcal{X} \rightarrow [0, 1]$ to distinguish

²Note that $\mathcal{P}_T = \mathcal{P}_{X_i|A_i=1}$, so that the target ATE on \mathcal{P}_T is in fact the ATT (ATE on the treated). This explains why our IPW estimator in Equation (6) differs from the classical IPW estimator.

members from non-members, yielding an estimate of the probability that any $x \in \mathcal{X}$ is a member. This classifier can be instantiated using a wide range of models, including logistic regression, random forests, or deep neural networks. For high-dimensional modalities such as text or images, one can first map inputs to embeddings using a pretrained model, and then apply a simple probabilistic classifier (e.g., logistic regression or a shallow network) on top of these representations. In practice, member and non-member data can be split into two independent parts, one used in Algorithm 3 and one used to learn the classifier $\hat{\pi}$. Cross-fitting, which alternates the roles of these splits and averages the results, can be used to leverage all the data efficiently.

By construction, a well-trained propensity score model captures the distributional differences between the conditional feature distributions $X_i | A_i = 1$ and $X_i | A_i = 0$, assigning higher scores to regions of the feature space that are more characteristic of members than non-members. If $\hat{\pi}$ is an asymptotically consistent estimator of π , the estimators of the causal evaluation metrics will be asymptotically unbiased. Consistency is measured as

$$\Delta_{\hat{\pi}} = \mathbb{E} \left[\left| \frac{\pi(X_i)}{1-\pi(X_i)} - \frac{\hat{\pi}(X_i)}{1-\hat{\pi}(X_i)} \right| \mid A_i = 0, \hat{\pi} \right].$$

We say that $\hat{\pi}$ is ℓ^1 -consistent if $\Delta_{\hat{\pi}} \rightarrow 0$. The following assumption is necessary to ensure that for each data point $x \in \mathcal{D}_T$, we have a positive (and lower-bounded, as opposed to Assumption 6.1) probability of being observed in the non-member set. Theorem 6.4 then shows that if propensity scores are learned well-enough, the ATE for the loss-based attack is well estimated by $\hat{\tau}_{ATE}^{(IPW)}$.

Assumption 6.3. There exists $\eta > 0$ such that $\pi(x) \leq 1 - \eta$ and $\hat{\pi}(x) \leq 1 - \eta$ for all $x \in \text{supp}(\mathcal{P}_T)$.

Theorem 6.4. *Assume that $(X_i, A_i, Y_i)_{i \in [n]}$ are obtained using Algorithm 3 with $Y_i = \mathcal{L}(\theta, X_i)$, that Assumptions 6.1 and 6.3 hold, and that \mathcal{A} is α -error stable and β -uniform training stable. Assume outcomes Y_i are in $[0, 1]$ almost surely. Furthermore, assume that $\hat{\pi}$ is independent from $(X_i, A_i, Y_i)_{i \in [n]}$. Then, with probability $1 - Ce^{-t}$:*

$$|\hat{\tau}_{ATE}^{(IPW)} - \tau_{ATE}| = \mathcal{O} \left(\Delta_{\hat{\pi}} + \frac{1}{\eta} \sqrt{\frac{t}{n}} + \sqrt{nt\alpha^2} + \sqrt{nt\beta^2} \right).$$

Theorem 6.4 has the same overall structure as the one-run result (Theorem 5.4), up to two additional terms: the additive bias $\Delta_{\hat{\pi}}$ of the propensity score estimator, and the factor $1/\eta$. The presence of $1/\eta$ is expected: when η is close to zero, inverse-propensity weighting (IPW) estimators are known to become unstable.

In the presence of severe distribution shift leading to extreme propensity scores, alternative causal inference estimators can be used to mitigate this instability. Letting $\hat{\mu}_0$ be an outcome regression model that estimates conditional MIA

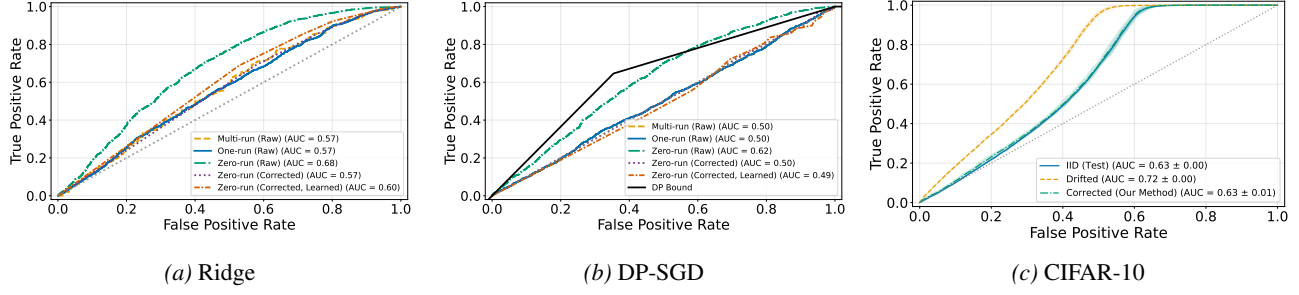


Figure 3. ROC curves and corresponding AUCs for different MIA evaluation scenarios. Figure 3a and Figure 3b: linear model trained on synthetic data, respectively with Ridge regression and DP-SGD. Figure 3c: ResNet model on CIFAR-10 data (averaged over 4 seeds).

response $\mu_0 : x \in \mathcal{X} \mapsto \mathbb{E}[Y_i(0)|X_i = x]$, the *G-Formula* estimator of the ATE (Wang et al., 2017) can be written as:

$$\hat{\tau}_{\text{ATE}}^{(\text{G})} = \frac{1}{n_1} \sum_{A_i=1} Y_i - \hat{\mu}_0(X_i). \quad (7)$$

The outcome regression model $\hat{\mu}_0$ is typically learned by fitting a regression of Y_i on X_i using non-member data points (i.e., those with $A_i = 0$). *Augmented Inverse Probability Weighting* (AIPW) combines the strengths of IPW and G-Formula estimators by incorporating both propensity score and outcome regression models (Shu & Tan, 2018):

$$\hat{\tau}_{\text{ATE}}^{(\text{AIPW})} = \hat{\tau}_{\text{ATE}}^{(\text{G})} - \frac{1}{n_1} \sum_{i=1}^n \frac{(1-A_i)\hat{\pi}(X_i)}{1-\hat{\pi}(X_i)} (Y_i - \hat{\mu}_0(X_i)). \quad (8)$$

The AIPW estimator is *doubly robust*, meaning it is consistent if either the propensity score model or the outcome regression is correctly specified. Although they are more robust to extreme propensity scores, G-Formula and AIPW still require Assumptions 6.1 and 6.3 to hold. Appendix D generalizes these two estimators to other causal metrics.

In summary, our results offer practical strategies to debias MIA evaluation in the zero-run regime, requiring only the training of a binary classifier and/or outcome regressors.

7. Experiments

Synthetic data. We consider linear regression trained on 2000 samples $X_i = (a_i, b_i)$ with $a_i \sim \mathcal{N}(0, I_d)$ and $b_i | a_i \sim \mathcal{N}(a_i^\top w_*, 1)$. We study two training algorithms: overparameterized ridge regression ($d = 2500$) and underparameterized DP-SGD ($d = 400$). Both satisfy error stability and uniform training stability. We evaluate a loss-based MIA under three regimes. (*Multi-run*) We fix a reference training set of 2000 points and sample 400 evaluation points. We train 400 models, one per evaluation point, with half of the training sets including the evaluation point and half excluding it. (*One-run*) We perform a single training on 2000 members and evaluate on these points and on 2000 non-members drawn i.i.d. from the same distribution. (*Zero-run*) We again perform a single training on 2000 members, but evaluate on 2000 non-members

drawn from a shifted distribution with $a_i \sim \mathcal{N}(\mu, I_d)$. Propensity scores are estimated via logistic regression.

ROC curves and AUCs are reported in Figures 3a and 3b. Multi-run and one-run evaluations nearly coincide, as interference are negligible in this case, while naive zero-run evaluation overestimates MIA performance due to distribution shift. After propensity-score correction, zero-run ROC and AUC align with non-shifted baselines. For DP-SGD, naive zero-run evaluation violates the theoretical ROC upper bound implied by (ε, δ) -DP (Dong et al., 2022), while corrected evaluation respects it, highlighting the importance of debiasing. Details about the experiments and results for other evaluation metrics can be found in Appendix G.1.

CIFAR-10. We perform zero-run evaluation on CIFAR-10 (Krizhevsky et al., 2009) using a ResNet-16 model. Members are drawn from a mixture of clean and noisy images (90%/10%), non-members from the reverse mixture (10%/90%). This ensures significant covariate shift while satisfying overlap. Propensity scores are estimated by fine-tuning an ImageNet-pretrained ResNet classifier. Additional experimental details are given in Appendix G.

Figure 3c shows ROC curves and AUCs for a loss-based MIA. Naive zero-run evaluation inflates attack performance ($\text{AUC} \approx 0.75$) due to distribution shift, misleadingly suggesting high memorization. Propensity-score correction recovers the true causal signal ($\text{AUC} \approx 0.66$), closely matching an IID baseline where non-members are drawn from the same mixture as members ($\text{AUC} \approx 0.65$), confirming that our method removes bias.

8. Related Work

Limits of the one-run regime. Recent work has studied the fundamental limits of the one-run regime for auditing differential privacy (DP) guarantees (Keinan et al., 2025; Xiang et al., 2025). These studies, like ours, trace the key limitation to interference between data points. Beyond this shared root cause, the objectives and conceptual frameworks differ: the prior work focuses on establishing DP lower bounds using

information-theoretic perspectives such as bit transmission or hypothesis testing, whereas we focus on evaluating MIAs, adopt a causal framing that explicitly captures how interference can invalidate counterfactual reasoning, and propose solutions to mitigate these limitations.

Formalizing and addressing MIA bias. MIAs are traditionally framed as randomized privacy games (Ye et al., 2022; Salem et al., 2023). However, unlike our causal framework, these games fail to capture the interference and distribution shifts characteristic of the one-run and zero-run regimes (Meeus et al., 2024b). Focusing on distribution shift in MIA evaluation for LLMs, Meeus et al. (2024b) suggest potential solutions, but these require intervention priors or during training (e.g., randomized train/test splits or data injection) or rely on heuristics. Kazmi et al. (2024) propose using synthetic data points from a generative model trained on the member data as non-members, but this approach is costly, data-hungry, and difficult to evaluate. While they provide theoretical conditions for obtaining meaningful DP lower bounds, their method offers no guarantees for MIA performance estimates. Eichler et al. (2025) develops techniques to mitigate distribution shift in post-hoc text data, yet offer no formal guarantees for the resulting MIA estimates. In contrast, we provide principled, causally valid estimators that rely only on simple binary classifiers or regressors.

Zhang et al. (2024) argue that several alternative techniques can be used to demonstrate to a third party that a model was trained on their data when the training set is unknown and re-training is impractical, including data watermarking (Sablayrolles et al., 2020; Kirchenbauer et al., 2024), random canary insertion (Carlini et al., 2019), and data reconstruction attacks (Carlini et al., 2021; Nasr et al., 2023a). The first two approaches require proactive intervention and trust in the model provider, while data reconstruction is fundamentally more difficult than membership inference. Developing statistically valid post-hoc MIA evaluations that do not rely on model provider cooperation or trust—the focus of our work—thus remains an important and practically relevant problem.

Causality and MIAs. We mention two prior works at the intersection of MIAs and causality, though orthogonal to our focus. Tople et al. (2020) show that causal learning can effectively reduce MIA success: unlike predictive models that may exploit spurious correlations, causal models rely on stable, invariant relationships between input and features outcomes. Baluta et al. (2022) use causal reasoning to investigate whether MIA performance arises solely from imperfect generalization, as suggested by prior work (Yeom et al., 2018; Sablayrolles et al., 2019). They find that while overfitting contributes to MIA success, it is in fact driven by a complex interplay of multiple factors.

Causal inference under interference. Seminal work formalized causal inference with interference via exposure

maps (Sobel, 2006; Hudgens & Halloran, 2008; Manski, 2013), which describe how each unit’s outcome depends on other units’ treatment assignments. These mappings are often represented by a graph, whose edges encode potential interference. Subsequent work has largely focused on fixed and sparse exposure maps (Bhattacharya et al., 2020; Papadogeorgou et al., 2019; Ogburn et al., 2024), with extensions to random (Clark & Handcock, 2021; Li & Wager, 2022), weighted (Forastiere et al., 2024), and dense (Miles et al., 2019) settings. In these frameworks, estimands are typically direct or indirect effects defined conditional on an observed exposure map. In contrast, interference in our setting is dense, unobserved, and arises as a random function of the covariates X_i through the training algorithm \mathcal{A} , which acts as a mediator (Figure 2). Rather than observing or modeling the exposure map directly, we impose assumptions on the mediator itself, leveraging learning-theoretic bounds on the influence of individual training points on the model’s behavior at other points. As a result, our estimands are not conditioned on a particular exposure map: τ_{ATE} averages over realizations of the mediator \mathcal{A} , and thus over the induced interference patterns. Together, our mediator-induced interference model, the unconditional estimands, and the mild assumptions we impose distinguish our setting from existing work and make Theorem 5.4 independently interesting within the interference literature.

9. Conclusion

We introduced a causal framework for evaluating membership inference attacks (MIAs), providing principled, statistically valid estimators that account for interference and distribution shifts inherent to one-run and zero-run regimes. Our approach unifies the evaluation of MIAs under a causal lens, clarifies the root causes of bias, and enables practical post-hoc evaluation without relying on model provider trust.

While our focus in this work has been on population-level metrics for membership inference—evaluating expected memorization over a target population—it is also crucial to study how different subgroups or subpopulations may be differently affected by memorization (Carlini et al., 2022; Kulynych et al., 2022). In causal inference, this corresponds to estimating heterogeneous treatment effects (Wager & Athey, 2018). Our framework provides a foundation for developing principled, subgroup-level membership risk estimates, even in challenging one-run and zero-run regimes.

Moreover, the causal perspective we advocate can be extended to other classes of privacy attacks beyond MIAs. For instance, attribute inference attacks (Fredrikson et al., 2015), where an adversary infers sensitive attributes of training data given partial observations, also exhibit evaluation biases (Jayaraman & Evans, 2022) that could be mitigated by counterfactual reasoning.

Acknowledgements

Most of this work was conducted while LB was a member of PreMeDICaL team, Inria, Idesp, Inserm, Université de Montpellier. LB's work at EPFL is supported by an EPFL AI Center Postdoctoral Fellowship.

This work is partially supported by grant ANR-20-CE23-0015 (Project PRIDE), ANR 22-PECY-0002 IPOP (Interdisciplinary Project on Privacy) project of the Cybersecurity PEPR, and ANR-22-PESN-0014 project of the Digital Health PEPR under the France 2030 program. This work was performed using HPC resources from GENCI-IDRIS (Grant 2023-AD011014018R3).

References

Baluta, T., Shen, S., Hitarth, S., Tople, S., and Saxena, P. Membership inference attacks and generalization: A causal perspective. In *CCS*, 2022.

Barbero, F., Gu, X., Choquette-Choo, C. A., Sitawarin, C., Jagielski, M., Yona, I., Veličković, P., Shumailov, I., and Hayes, J. Extracting alignment data in open models. *arXiv preprint arXiv:2510.18554*, 2025.

Bertran, M., Tang, S., Roth, A., Kearns, M., Morgenstern, J. H., and Wu, S. Z. Scalable membership inference attacks via quantile regression. *Advances in Neural Information Processing Systems*, 36:314–330, 2023.

Bhattacharya, R., Malinsky, D., and Shpitser, I. Causal inference under interference and network uncertainty. In *Uncertainty in Artificial Intelligence*, pp. 1028–1038. PMLR, 2020.

Bousquet, O. and Elisseeff, A. Stability and generalization. *Journal of machine learning research*, 2(Mar):499–526, 2002.

Buyse, M. Generalized pairwise comparisons of prioritized outcomes in the two-sample problem. *Statistics in Medicine*, 29(30):3245–3257, dec 2010.

Carlini, N., Liu, C., Erlingsson, Ú., Kos, J., and Song, D. The secret sharer: Evaluating and testing unintended memorization in neural networks. In *28th USENIX security symposium (USENIX security 19)*, pp. 267–284, 2019.

Carlini, N., Tramer, F., Wallace, E., Jagielski, M., Herbert-Voss, A., Lee, K., Roberts, A., Brown, T., Song, D., Erlingsson, U., et al. Extracting training data from large language models. In *30th USENIX security symposium (USENIX Security 21)*, pp. 2633–2650, 2021.

Carlini, N., Chien, S., Nasr, M., Song, S., Terzis, A., and Tramer, F. Membership inference attacks from first principles. In *2022 IEEE symposium on security and privacy (SP)*, pp. 1897–1914. IEEE, 2022.

Cinelli, C., Feller, A., Imbens, G., Kennedy, E., Maglia-cane, S., and Zubizarreta, J. Challenges in statistics: A dozen challenges in causality and causal inference. *arXiv preprint arXiv:2508.17099*, 2025.

Clark, D. A. and Handcock, M. S. An approach to causal inference over stochastic networks. *arXiv preprint arXiv:2106.14145*, 2021.

Concord Music Group v. Anthropic. Concord Music Group, Inc. v. Anthropic PBC, 5:24-cv-03811 - CourtListener.com, 2023. URL <https://www.courtlistener.com/docket/68889092/concord-music-group-inc-v-anthropic-pbc/>.

Deng, J., Dong, W., Socher, R., Li, L.-J., Li, K., and Fei-Fei, L. Imagenet: A large-scale hierarchical image database. In *2009 IEEE Conference on Computer Vision and Pattern Recognition*, pp. 248–255, 2009. doi: 10.1109/CVPR.2009.5206848.

Dong, J., Roth, A., and Su, W. J. Gaussian differential privacy. *Journal of the Royal Statistical Society: Series B (Statistical Methodology)*, 84(1):3–37, 2022.

Duan, M., Suri, A., Miresghallah, N., Min, S., Shi, W., Zettlemoyer, L., Tsvetkov, Y., Choi, Y., Evans, D., and Hajishirzi, H. Do membership inference attacks work on large language models? In *Conference on Language Modeling (COLM)*, 2024.

Eichler, C., Champeil, N., Anciaux, N., Bensamoun, A., Arcolezi, H. H., and Fuentes, J. M. D. Nob-MIAs: Non-biased Membership Inference Attacks Assessment on Large Language Models with Ex-Post Dataset Construction. volume 15438, pp. 441–456. 2025. doi: 10.1007/978-981-96-0570-5_32. URL <https://arxiv.org/abs/2408.05968>. arXiv:2408.05968 [cs].

European Data Protection Board. Opinion 28/2024 on certain data protection aspects related to the processing of personal data in the context of ai models, 2024. URL https://www.edpb.europa.eu/our-work-tools/our-documents/opinion-board-art-64/opinion-282024-certain-data-protection-aspects_en.

Even, M. and Josse, J. Rethinking the win ratio: A causal framework for hierarchical outcome analysis, 2025. URL <https://arxiv.org/abs/2501.16933>.

Forastiere, L., Del Prete, D., and Sciabolazza, V. L. Causal inference on networks under continuous treatment interference. *Social Networks*, 76:88–111, 2024.

Fredrikson, M., Jha, S., and Ristenpart, T. Model inversion attacks that exploit confidence information and basic countermeasures. In *CCS*, 2015.

Hardt, M., Recht, B., and Singer, Y. Train faster, generalize better: Stability of stochastic gradient descent. In *International conference on machine learning*, pp. 1225–1234. PMLR, 2016.

Hayes, J., Shumailov, I., Choquette-Choo, C. A., Jagielski, M., Kaassis, G., Lee, K., Nasr, M., Ghalebikesabi, S., Miresghallah, N., Sundaram Mutu Selva Annamalai, M., et al. Strong membership inference attacks on massive datasets and (moderately) large language models. *arXiv e-prints*, pp. arXiv–2505, 2025.

He, K., Zhang, X., Ren, S., and Sun, J. Deep residual learning for image recognition. In *2016 IEEE Conference on Computer Vision and Pattern Recognition (CVPR)*, 2016.

Hernán, M. A. and Robins, J. M. Causal inference, 2010.

Hudgens, M. G. and Halloran, M. E. Toward causal inference with interference. *Journal of the american statistical association*, 103(482):832–842, 2008.

Imbens, G. W. and Rubin, D. B. *Causal Inference in Statistics, Social, and Biomedical Sciences*. Cambridge University Press, Cambridge, UK, 2015. ISBN 978-0521885881.

Jagielski, M., Ullman, J., and Oprea, A. Auditing differentially private machine learning: How private is private sgd? *Advances in Neural Information Processing Systems*, 33:22205–22216, 2020.

Jayaraman, B. and Evans, D. Are attribute inference attacks just imputation? In *PCCS*, 2022.

Kazmi, M., Lautraite, H., Akbari, A., Tang, Q., Soroco, M., Wang, T., Gambs, S., and Lécuyer, M. Panoramia: Privacy auditing of machine learning models without retraining. *Advances in Neural Information Processing Systems*, 37:57262–57300, 2024.

Keinan, A., Shenfeld, M., and Ligett, K. How well can differential privacy be audited in one run? In *The Thirty-ninth Annual Conference on Neural Information Processing Systems*, 2025. URL <https://openreview.net/forum?id=004uT1Sufe>.

Kirchenbauer, J., Geiping, J., Wen, Y., Katz, J., Miers, I., and Goldstein, T. A Watermark for Large Language Models, May 2024. URL <http://arxiv.org/abs/2301.10226>. arXiv:2301.10226 [cs].

Krizhevsky, A. et al. Learning multiple layers of features from tiny images. 2009.

Kulynych, B., Yaghini, M., Cherubin, G., Veale, M., and Troncoso, C. Disparate vulnerability to membership inference attacks. *Proc. Priv. Enhancing Technol.*, 2022(1): 460–480, 2022.

Li, S. and Wager, S. Random graph asymptotics for treatment effect estimation under network interference. *The Annals of Statistics*, 50(4):2334–2358, 2022.

Liu, T., Boglioni, M., Fu, Y., Hu, S., Thaker, P., and Wu, Z. S. Enhancing One-run Privacy Auditing with Quantile Regression-Based Membership Inference. *arXiv preprint arXiv:2506:15349*, 2025.

Mahloujifar, S., Melis, L., and Chaudhuri, K. Auditing f -differential privacy in one run. *arXiv preprint arXiv:2410.22235*, 2024.

Maini, P., Yaghini, M., and Papernot, N. Dataset Inference: Ownership Resolution in Machine Learning, April 2021. URL <http://arxiv.org/abs/2104.10706>. arXiv:2104.10706 [stat].

Maini, P., Jia, H., Papernot, N., and Dziedzic, A. LLM Dataset Inference: Did you train on my dataset? 2024.

Mann, H. B. and Whitney, D. R. On a test of whether one of two random variables is stochastically larger than the other. *The Annals of Mathematical Statistics*, 18(1): 50–60, mar 1947. ISSN 0003-4851.

Manski, C. F. Identification of treatment response with social interactions. *The Econometrics Journal*, 16(1): S1–S23, 2013.

Mao, L. On causal estimation using u -statistics. *Biometrika*, 105(1):215–220, dec 2017. ISSN 1464-3510.

Mattern, J., Miresghallah, F., Jin, Z., Schölkopf, B., Sachan, M., and Berg-Kirkpatrick, T. Membership inference attacks against language models via neighbourhood comparison. In Rogers, A., Boyd-Graber, J., and Okazaki, N. (eds.), *Findings of the Association for Computational Linguistics: ACL 2023*, pp. 11330–11343, Toronto, Canada, July 2023. Association for Computational Linguistics. doi: 10.18653/v1/2023.findings-acl.719. URL <https://aclanthology.org/2023.findings-acl.719/>.

Meeus, M., Jain, S., Rei, M., and de Montjoye, Y.-A. Did the neurons read your book? document-level membership inference for large language models. In *33rd USENIX Security Symposium (USENIX Security 24)*, pp. 2369–2385, 2024a.

Meeus, M., Shilov, I., Jain, S., Faysse, M., Rei, M., and de Montjoye, Y.-A. Sok: Membership inference attacks on llms are rushing nowhere (and how to fix it). *arXiv preprint arXiv:2406.17975*, 2024b.

Miles, C. H., Petersen, M., and van der Laan, M. J. Causal inference when counterfactuals depend on the proportion of all subjects exposed. *Biometrics*, 75(3):768–777, 2019.

Nasr, M., Carlini, N., Hayase, J., Jagielski, M., Cooper, A. F., Ippolito, D., Choquette-Choo, C. A., Wallace, E., Tramèr, F., and Lee, K. Scalable extraction of training data from (production) language models. *arXiv preprint arXiv:2311.17035*, 2023a.

Nasr, M., Hayes, J., Steinke, T., Balle, B., Tramèr, F., Jagielski, M., Carlini, N., and Terzis, A. Tight auditing of differentially private machine learning. In *32nd USENIX Security Symposium (USENIX Security 23)*, pp. 1631–1648, 2023b.

New York Times v. OpenAI. NYT v. OpenAI: The Times’s About-Face, 2023. URL <https://harvardlawreview.org/blog/2024/04/nyt-v-openai-the-timess-about-face/>.

Ogburn, E. L., Sofrygin, O., Diaz, I., and Van der Laan, M. J. Causal inference for social network data. *Journal of the American Statistical Association*, 119(545):597–611, 2024.

Papadogeorgou, G., Mealli, F., and Zigler, C. M. Causal inference with interfering units for cluster and population level treatment allocation programs. *Biometrics*, 75(3):778–787, 2019.

Pitcan, Y. A note on concentration inequalities for U -statistics. *arXiv preprint arXiv:1712.06160*, 2017.

Pocock, S. J., Ariti, C. A., Collier, T. J., and Wang, D. The win ratio: a new approach to the analysis of composite endpoints in clinical trials based on clinical priorities. *European Heart Journal*, 33(2):176–182, sep 2011. ISSN 1522-9645.

Rosenbaum, P. R. and Rubin, D. B. The central role of the propensity score in observational studies for causal effects. *Biometrika*, 70(1):41–55, 1983.

Rubin, D. B. Estimating causal effects of treatments in randomized and nonrandomized studies. *Journal of educational Psychology*, 66(5):688, 1974.

Sablayrolles, A., Douze, M., Ollivier, Y., Schmid, C., and Jégou, H. White-box vs black-box: Bayes optimal strategies for membership inference. In *ICML*, 2019.

Sablayrolles, A., Douze, M., Schmid, C., and Jégou, H. Radioactive data: tracing through training, February 2020. URL <http://arxiv.org/abs/2002.00937>. arXiv:2002.00937 [stat].

Salem, A., Cherubin, G., Evans, D., Kopf, B., Paverd, A., Suri, A., Tople, S., and Zanella-Beguelin, S. SoK: Let the Privacy Games Begin! A Unified Treatment of Data Inference Privacy in Machine Learning . In *IEEE Symposium on Security and Privacy (S&P)*, 2023.

Shi, W., Ajith, A., Xia, M., Huang, Y., Liu, D., Blevins, T., Chen, D., and Zettlemoyer, L. Detecting pretraining data from large language models. *arXiv preprint arXiv:2310.16789*, 2023.

Shokri, R., Stronati, M., Song, C., and Shmatikov, V. Membership inference attacks against machine learning models. In *2017 IEEE symposium on security and privacy (SP)*, pp. 3–18. IEEE, 2017.

Shu, H. and Tan, Z. Improved estimation of average treatment effects on the treated: Local efficiency, double robustness, and beyond. *arXiv preprint arXiv:1808.01408*, 2018.

Sobel, M. E. What do randomized studies of housing mobility demonstrate? causal inference in the face of interference. *Journal of the American Statistical Association*, 101(476):1398–1407, 2006.

Splawa-Neyman, J., Dabrowska, D. M., and Speed, T. P. On the application of probability theory to agricultural experiments. essay on principles. section 9. *Statistical Science*, pp. 465–472, 1990.

Steinke, T., Nasr, M., and Jagielski, M. Privacy auditing with one (1) training run. *Advances in Neural Information Processing Systems*, 36:49268–49280, 2023.

Tian, J. and Pearl, J. Probabilities of causation: Bounds and identification. *Annals of Mathematics and Artificial Intelligence*, 28(1):287–313, 2000.

Tople, S., Sharma, A., and Nori, A. Alleviating privacy attacks via causal learning. In *International Conference on Machine Learning*, pp. 9537–9547. PMLR, 2020.

Wager, S. Causal inference: A statistical learning approach, 2024.

Wager, S. and Athey, S. Estimation and inference of heterogeneous treatment effects using random forests. *Journal of the American Statistical Association*, 113(523):1228–1242, 2018.

Wang, A., Nianogo, R. A., and Arah, O. A. G-computation of average treatment effects on the treated and the untreated. *BMC medical research methodology*, 17(1):3, 2017.

Wilcoxon, F. Individual comparisons by ranking methods. *Biometrics Bulletin*, 1(6):80, dec 1945. ISSN 0099-4987.

Xiang, Z., Wang, T., and Wang, D. Privacy audit as bits transmission: (im)possibilities for audit by one run. In *Proceedings of the 34th USENIX Conference on Security Symposium*, 2025.

Ye, J., Maddi, A., Murakonda, S. K., Bindschaedler, V., and Shokri, R. Enhanced membership inference attacks against machine learning models. In *CCS*, 2022.

Yeom, S., Giacomelli, I., Fredrikson, M., and Jha, S. Privacy risk in machine learning: Analyzing the connection to overfitting. In *2018 IEEE 31st computer security foundations symposium (CSF)*, pp. 268–282. IEEE, 2018.

Zarifzadeh, S., Liu, P., and Shokri, R. Low-cost high-power membership inference attacks. In *Forty-first International Conference on Machine Learning, ICML 2024, Vienna, Austria, July 21-27, 2024*. OpenReview.net, 2024. URL <https://openreview.net/forum?id=sT7UJh5CTc>.

Zhang, J., Das, D., Kamath, G., and Tramèr, F. Membership inference attacks cannot prove that a model was trained on your data. *arXiv preprint arXiv:2409.19798*, 2024.

A. Additional Causal Inference Details

A.1. Causal Inference Assumptions

We here explain the different regimes used in causal inference to estimate treatment effects. In particular, we explicit the underlying assumptions that are made in these regimes.

Randomized Control Trial (RCT). In RCTs, treatment is randomized and there are no interferences. Assumption 2.1 is thus assumed to hold with 2. (a) for assignment mechanism. The overlap assumption holds, since $\mathbb{P}(A_i = 1 | X_i) = \mathbb{P}(A_i = 1)$ does not depend on the covariates. The SUTVA assumption means that there are no interferences, and is usually made for RCTs.

Observational Studies. RCTs are usually expensive and have restrictive eligibility criteria, hindering both their statistical power (smaller samples) and their population. As a consequence, the promise of observational data through the use of hospital electronic health records has emerged (Rosenbaum & Rubin, 1983). However this comes at the cost of non-randomized treatment assignments, and estimating treatment effects on observational data is infeasible without additional structural assumption. As a consequence, if there are no interferences or if they are neglected, Assumption 2.1 is assumed to hold with 2. (b) for the assignment mechanism: the observed covariates X_i are rich enough, so that there are no unobserved confounders. The overlap assumption is assumed to hold here, and does not hold by design as in RCTs: given covariates X_i , the probability of patient i of being treated is bounded away from 0 and 1.

RCT with Interferences. For vaccine trials for instance, the SUTVA assumption can no longer be made, due to herd immunity. As a consequence, it is replaced using the interference formalism introduced in Section 2.2 as follows.

Assumption A.1 (Assumptions under interference).

1. (Interference) $Y_i = Y_i(\bar{A})$;
2. (Generalized Unconfoundedness) $\bar{A} \perp\!\!\!\perp \{\bar{Y}(\bar{a})\}_{\bar{a}}$;
3. (Generalized Overlap) For all $i \neq j$,

$$0 < \mathbb{P}(A_i = a | \bar{A}_{-i}) < 1.$$

Observational Studies with Interferences. Combining both difficulties (confounders and interferences), such as vaccine observational data, requires making the following assumption.

Assumption A.2 (Interference and confounders).

1. (Interference) $Y_i = Y_i(\bar{A})$;
2. (Conditional Generalized Unconfoundedness) $\bar{A} \perp\!\!\!\perp \{\bar{Y}(\bar{a})\}_{\bar{a}} | \bar{X}$;
3. (Conditional Generalized Overlap) For all $i \neq j$,

$$0 < \mathbb{P}(A_i = a | \bar{X}, \bar{A}_{-i}) < 1 \text{ a.s.}$$

A.2. Discussion on the Causal AUC

The classical AUC compares the scores of outcomes for treated ($A_i = 1$) and control ($A_i = 0$) datapoints, and can be expressed as:

$$\mathbb{P}(Y_i \geq Y_j | A_i = 1, A_j = 0).$$

It is however not straightforward to write the causal AUC, defined as the area under the causal ROC curve, as a comparison estimand. In causal inference, the most common quantity for comparing potential outcomes is the probability of necessity and sufficiency (PNS) (Tian & Pearl, 2000), defined as $\text{PNS} = \mathbb{P}(Y_i(1) > Y_i(0))$. This represents the probability that a given datapoint has a higher score if treated compared to not being treated. While PNS is useful for assessing treatment effectiveness, it is unidentifiable in practice. Instead, the Mann-Whitney-Wilcoxon test statistics (Wilcoxon, 1945; Mann & Whitney, 1947), along with other pairwise comparison methods like the Win Ratio or Net Benefit (Pocock et al., 2011;

Buyse, 2010; Mao, 2017; Even & Josse, 2025), estimate an identifiable quantity known as the *Win Proportion* (WP), given by:

$$\text{WP} \stackrel{\text{def}}{=} \mathbb{P}(Y_i(1) > Y_j(0) \mid A_i = A_j = 1), .$$

This estimand is a causal interpretation of the AUC, replacing the unknown counterfactual with that of another datapoint, making it identifiable under standard causal assumptions. However, the WP is not well-defined in the presence of interference, which makes it unidentifiable. In the one-run and zero-run settings, the joint distribution of $(Y_i(1), Y_j(0))$ becomes unidentifiable because changes in A_i or A_j (due to datapoint insertions) affect the potential outcomes $Y_i(1)$ and $Y_j(0)$. Therefore, a Causal Comparison AUC can be defined as follows using causal inference with interference notations.

Definition A.3 (Causal Comparison AUC). For $i \neq j$, and $a_i, a_j \in \{0, 1\}$, define $Y_{i,j}(a_i, a_j)$ as $Y_{i,j}(a_i, a_j) =$

$$Y_i(A_1, \dots, A_{i-1}, a_i, A_{i+1}, \dots, A_{j-1}, a_j, A_{j+1}, \dots, A_n).$$

We then define the causal AUC as:

$$\tilde{\tau}_{\text{AUC}} \stackrel{\text{def}}{=} \mathbb{P}(Y_{i,j}(1, 0) > Y_{j,i}(0, 1) \mid A_i = A_j = 1) .$$

Importantly, note that if SUTVA holds (no interferences, $Y_i(\bar{a}) = Y_i(a_i)$ for any $\bar{a} \in \{0, 1\}^n$) we have $Y_{i,j}(a_i, a_j) = Y_i(a_i)$ and $\tilde{\tau}_{\text{AUC}} = \text{WP}$. Definition A.3 is thus a strict generalization of the WP estimand to the interference setting. Under interferences, $\tilde{\tau}_{\text{AUC}}$ is however in general not identifiable, even under Assumption A.1 or Assumption A.2, that would instead need to be replaced by the following (interference observational setting).

Assumption A.4 (Alternative assumption).

1. (Interference) $Y_i = Y_i(\bar{A})$;
2. (Conditional Generalized Unconfoundedness) $\bar{A} \perp\!\!\!\perp \{\bar{Y}(\bar{a})\}_{\bar{a}} \mid \bar{X}$;
3. (Conditional Generalized Overlap) For all $i \neq j$,

$$0 < \mathbb{P}(A_i = a, A_j = a' \mid \bar{X}, \bar{A}_{-(i,j)}) < 1 \text{ a.s.}$$

A.3. Identifiability Proofs

The proofs of the ATE parts of Propositions 4.1, 5.1 and 6.2 are all implied by the following.

Proposition A.5. *Assume that Assumption A.2 holds. Then:*

$$\tau_{\text{ATE}} = \frac{\mathbb{E}[A_i Y_i]}{\mathbb{P}(A_i = 1)} - \frac{\mathbb{E}\left[\frac{\pi(X_i)(1-A_i)}{1-\pi(X_i)} Y_i\right]}{\mathbb{P}(A_i = 0)} . \quad (9)$$

Proposition A.5 implies Proposition 6.2 since under Assumption 6.1 we have that Assumption A.2 holds in the Zero-run setting. Then, in the One-run and Multi-run settings, Assumptions 2.1 and A.1 respectively hold, which implies Assumption A.2 and thus Proposition A.5. Then specifying Proposition A.5 in the One-run setting for which π is constant equal to 0.5, we get the ATE parts of Propositions 4.1 and 5.1. Identification for the other causal metrics follow from similar arguments.

Proof of Proposition A.5. Under the assumptions of either of Propositions 4.1, 5.1 and 6.2, we have that Assumption A.2 holds. First,

$$\begin{aligned} \mathbb{E}_{\mathcal{P}_T}[Y_i(1)] &= \mathbb{E}[Y_i(1) \mid A_i = 1] \\ &= \mathbb{E}[Y_i \mid A_i = 1] \quad (\text{Interference assumption in Assumption A.2}) \\ &= \mathbb{E}[A_i Y_i \mid A_i = 1] . \end{aligned}$$

Then,

$$\begin{aligned} \mathbb{E}[A_i Y_i] &= \mathbb{E}[A_i Y_i \mid A_i = 1] \mathbb{P}(A_i = 1) + \mathbb{E}[A_i Y_i \mid A_i = 0] \mathbb{P}(A_i = 0) \\ &= \mathbb{E}[A_i Y_i \mid A_i = 1] \mathbb{P}(A_i = 1) + 0 , \end{aligned}$$

leading to $\mathbb{E}_{\mathcal{P}_T}[Y_i(1)] = \frac{\mathbb{E}[A_i Y_i]}{\mathbb{P}(A_i=1)}$. For the other term,

$$\begin{aligned}
 \mathbb{E}_{\mathcal{P}_T}[Y_i(0)] &= \mathbb{E}[Y_i(0)|X_i \sim \mathcal{P}_T] \\
 &= \mathbb{E}[\mathbb{E}[Y_i(0)|\bar{X}]|X_i \sim \mathcal{P}_T] \\
 &= \mathbb{E}[\mathbb{E}[Y_i(0)|\bar{X}, \bar{A}_{-i}, A_i = 0]|X_i \sim \mathcal{P}_T] \quad (\text{Conditional Generalized Unconfoundedness}) \\
 &= \mathbb{E}[\mathbb{E}[Y_i|\bar{X}, \bar{A}_{-i}, A_i = 0]|X_i \sim \mathcal{P}_T] \quad (\text{Interference assumption in Assumption A.2}) \\
 &= \mathbb{E}[\mathbb{E}[Y_i|X_i, A_i = 0]|X_i \sim \mathcal{P}_T] \\
 &= \mathbb{E}[\mathbb{E}[(1 - A_i)Y_i|X_i, A_i = 0]|X_i \sim \mathcal{P}_T].
 \end{aligned}$$

Now,

$$\begin{aligned}
 \mathbb{E}[(1 - A_i)Y_i|X_i] &= \mathbb{E}[(1 - A_i)Y_i|X_i, A_i = 0]\mathbb{P}((1 - A_i)A_i = 0|X_i) + \mathbb{E}[(1 - A_i)Y_i|X_i, A_i = 1]\mathbb{P}(A_i = 1|X_i) \\
 &= \mathbb{E}[(1 - A_i)Y_i|X_i, A_i = 0](1 - \pi(X_i)) + 0.
 \end{aligned}$$

This leads to:

$$\begin{aligned}
 \mathbb{E}_{\mathcal{P}_T}[Y_i(0)] &= \mathbb{E}[\mathbb{E}[(1 - A_i)Y_i|X_i](1 - \pi(X_i))^{-1}|X_i \sim \mathcal{P}_T] \\
 &= \mathbb{E}[g(X_i)|X_i \sim \mathcal{P}_T].
 \end{aligned}$$

with $g(x) = \mathbb{E}[(1 - A_i)Y_i|X_i = x](1 - \pi(x))^{-1}$. Now, notice that the density of \mathcal{P}_T with respect to \mathcal{P}_{X_i} is proportional to π : $\frac{d\mathcal{P}_T(x)}{d\mathcal{P}_{X_i}}(x) = \frac{\pi(x)}{\mathbb{P}(A_i=1)}$. Thus, $\mathbb{E}[g(X_i)|X_i \sim \mathcal{P}_T] = \mathbb{E}\left[\frac{\pi(X_i)}{\mathbb{P}(A_i=1)}g(X_i)|X_i \sim \mathcal{P}_{X_i}\right]$, concluding the proof. \square

B. Results in the underparametrized regime

Next theorem shows that when the number of samples becomes large in front of the dimension of the model, MIAs based on the loss cannot recover any signal.

Theorem B.1 (Underparametrized Regime). *Consider the assumptions of Theorem 5.4 but without uniform training stability. Further assume that $\theta = \mathcal{A}(\mathcal{D}) \in \mathbb{R}^D$ has norm almost surely bounded by a constant B and that $\theta \mapsto \mathcal{L}(\theta, x)$ is L -Lipschitz for all $x \in \mathcal{X}$. Then:*

$$|\tau_{\text{ATE}}| = \mathcal{O}\left(\sqrt{n \log(n) \alpha^2} + \sqrt{\frac{D \log(BL_n)}{n}}\right).$$

C. Estimators for and generalization to all Causal MIA Evaluation Metrics

C.1. Multi-run setting

Estimators of the other causal metrics beyond the ATE in the multi-run setting write as:

$$\begin{aligned}
 \hat{\tau}_{\text{ATE}} &= \frac{1}{n_1} \sum_{i:A_i=1} Y_i - \frac{1}{n_0} \sum_{i:A_i=0} Y_i, \\
 \hat{\tau}_{\text{TPR}}(t) &= \frac{1}{n_1} \sum_{i:A_i=1} \mathbb{1}_{\{Y_i \geq t\}} \\
 \hat{\tau}_{\text{FPR}}(t) &= \frac{1}{n_0} \sum_{i:A_i=0} \mathbb{1}_{\{Y_i \geq t\}} \\
 \hat{\tau}_{\text{AUC}} &= \frac{1}{n_1 n_0} \sum_{(i,j):(A_i,A_j)=(1,0)} \mathbb{1}_{\{Y_i > Y_j\}}, \\
 \hat{\tau}_{\text{TPR@FPR}}(\alpha) &= \frac{1}{n_1} \sum_{i:A_i=1} \mathbb{1}_{\{Y_i \geq \hat{t}_\alpha\}},
 \end{aligned} \tag{10}$$

where \hat{t}_α is an estimator of the $1 - \alpha$ quantile of $\{Y_i : A_i = 0\}$, of respectively the ATE (causal membership advantage), the causal TPR and FPR at threshold $t \in \mathbb{R}$, the causal AUC and the causal TPR at fixed FPR $\alpha \in (0, 1)$.

Proposition C.1. Assume that $(X_i, A_i, Y_i)_{i \in [n]}$ is obtained in the Multi Run setting (Algorithm 1). Then, $\hat{\tau}_{ATE}$, $\hat{\tau}_{ATE}(t)$ for $t \in \mathbb{R}$ and $\hat{\tau}_{AUC}$ are consistent estimators of τ_{ATE} , $\tau_{ATE}(t)$ and τ_{AUC} . If $t \mapsto FPR(t)$ is continuous, $\hat{\tau}_{TPR@FPR}(\alpha)$ is a consistent estimator of $\tau_{TPR@FPR}(\alpha)$ for $\alpha \in [0, 1]$.

Moving beyond consistency, non-asymptotic rates can be obtained directly from the difference in means estimator properties (Wager, 2024, e.g.). For $\hat{\tau}_{TPR}(t)$, with probability $1 - 4e^{-\lambda}$,

$$|\hat{\tau}_{TPR}(t) - \tau_{TPR}(t)| \leq \sqrt{\frac{\lambda}{2n_1}} + \sqrt{\frac{\lambda}{2n_0}},$$

and similarly for τ_{TPR} , while for the causal membership advantage (ATE) if outcomes Y_i are bounded by a constant B :

$$|\hat{\tau}_{ATE} - \tau_{ATE}| \leq B\sqrt{\frac{2\lambda}{n_1}} + B\sqrt{\frac{2\lambda}{n_0}}.$$

Non-asymptotic results for the causal AUC can be obtained via U -statistics (Pitcan, 2017).

C.2. One-run setting

In the one-run setting, the estimators of the different causal evaluation metrics are the same as in the multi-run (see Equation (10)), at the exception of the causal AUC estimator, which is now the area under the estimated causal ROC curve $\{(\hat{\tau}_{FPR}(t), \hat{\tau}_{TPR}(t))\}$.

C.3. Zero-run setting

In the zero-run setting, the estimators of the different causal evaluation metrics are now weighted with propensity scores as follows:

$$\begin{aligned} \hat{\tau}_{ATE}^{(IPW)} &= \frac{1}{n_1} \sum_{A_i=1} Y_i - \frac{1}{n_0} \sum_{A_i=0} \frac{\hat{\pi}(X_i)}{1 - \hat{\pi}(X_i)} Y_i, \\ \hat{\tau}_{TPR}^{(IPW)}(t) &= \frac{1}{n_1} \sum_{A_i=1} \mathbb{1}_{\{Y_i \geq t\}} \\ \hat{\tau}_{FPR}^{(IPW)}(t) &= \frac{1}{n_0} \sum_{A_i=0} \frac{\hat{\pi}(X_i)}{1 - \hat{\pi}(X_i)} \mathbb{1}_{\{Y_i \geq t\}} \\ \hat{\tau}_{TPR@FPR}^{(IPW)}(\alpha) &= \frac{1}{n_1} \sum_{A_i=1} Y_i \end{aligned} \tag{11}$$

with

$$\hat{t}_\alpha \in \operatorname{argmin} \left\{ t : \frac{1}{n_0} \sum_{A_i=1} \frac{\hat{\pi}(X_i)}{1 - \hat{\pi}(X_i)} \mathbb{1}_{\{Y_i \geq t\}} \geq 1 - \alpha \right\},$$

where $\hat{\pi} : \mathcal{X} \rightarrow [0, 1]$ is an estimator of the propensity score function π , learned on independent data. The estimator of the causal AUC is still the area under the estimated ROC curve. Next proposition then generalizes the identification result established in Proposition 6.2 to the other causal evaluation metrics.

Proposition C.2. Under Assumption 6.1, if $(X_i, A_i, Y_i)_{i \in [n]}$ are obtained according to Algorithm 3, the causal evaluation metrics are identifiable. Let the propensity score π write as:

$$\forall x \in \mathcal{X}, \quad \pi(x) \stackrel{\text{def}}{=} \mathbb{P}(A_i = 1 | X_i = x).$$

We have:

$$\begin{aligned} \tau_{ATE} &= \mathbb{E}[A_i Y_i] \mathbb{P}(A_i = 1)^{-1} \\ &\quad - \mathbb{E}\left[\frac{\pi(X_i)(1 - A_i)}{1 - \pi(X_i)} Y_i\right] \mathbb{P}(A_i = 0)^{-1}, \\ \tau_{TPR}(t) &= \mathbb{E}[A_i \mathbb{1}_{\{Y_i \geq t\}}] \mathbb{P}(A_i = 1)^{-1} \\ \tau_{FPR}(t) &= \mathbb{E}\left[\frac{\pi(X_i)(1 - A_i)}{1 - \pi(X_i)} \mathbb{1}_{\{Y_i \geq t\}}\right] \mathbb{P}(A_i = 0)^{-1}. \end{aligned}$$

D. G-Formula and AIPW beyond the ATE

Letting $\hat{\mu}_0$ be a regression model that estimates conditional MIA response $\mu_0 : x \in \mathcal{X} \mapsto \mathbb{E}[Y_i(0)|X_i = x]$, the G-Formula estimator of the ATE (which is in fact an ATT) is defined in Equation (7). Outcome regression model $\hat{\mu}_0$ is typically learned on an independent dataset or using crossfitting, by fitting a model $Y_i \sim X_i$ on non-member datapoints (satisfying $A_i = 0$). We now generalize this approach to the causal TPR and FPR, in order to obtain a causal ROC curve and a causal AUC, without having to resort to propensity scores.

TPR. For the causal TPR, the G-Formula estimator $\hat{\tau}_{\text{TPR}}^{(\text{G})}(t)$ is unchanged (same as $\hat{\tau}_{\text{TPR}}^{(\text{IPW})}(t)$ in Equation (11)). The same for the AIPW estimator.

FPR. For the causal TPR, the G-Formula estimator $\hat{\tau}_{\text{FPR}}^{(\text{G})}(t)$ requires to learn a family of regressors $\{\hat{\mu}_{0,t}, t \in \mathbb{R}\}$ where $\hat{\mu}_{0,t}$ is an estimator of:

$$\mu_{0,t} : x \in \mathcal{X} \mapsto \mathbb{P}(Y_i(0) \geq t | X_i = x).$$

Since $\mu_{0,t}(x) = \mathbb{P}(Y_i \geq t | X_i = x, A_i = 0)$, $\hat{\mu}_{0,t}$ can be learned by using a classifier and outputting conditional probabilities, that we fit on the non-members $\{(X_i, \mathbb{1}_{\{Y_i \geq t\}}) | A_i = 0\}$. This needs to be done for all $t \in \mathbb{R}$ or for a discretized set. The causal FPR at threshold t can be estimated using:

$$\hat{\tau}_{\text{FPR}}^{(\text{G})}(t) = \frac{1}{n_1} \sum_{A_i=1} \hat{\mu}_{0,t}(X_i).$$

Another approach would be to use *distributional regression*, which is typical of comparison-based estimands in causal inference (Even & Josse, 2025). An estimator $\hat{\mathbb{P}}_0(x, \cdot)$ of the probability distribution $\mathbb{P}_{Y|X_i=x, A_i=0}$ could be learned, where $\hat{\mathbb{P}}(x, t)$ is an estimator of $\mathbb{P}(Y_i \geq t | X_i = x)$.

Finally, the AIPW estimator of the causal FPR writes as:

$$\hat{\tau}_{\text{FPR}}^{(\text{AIPW})}(t) = \frac{1}{n_1} \sum_{i=1}^n \left[A_i \hat{\mu}_{0,t}(X_i) - \frac{(1 - A_i) \hat{\pi}(X_i)}{1 - \hat{\pi}(X_i)} (\mathbb{1}_{\{Y_i \geq t\}} - \hat{\mu}_{0,t}(X_i)) \right]$$

E. Proofs in the 1-Run Randomized setting

In all the proofs, everything is done conditionally on the initial data \mathcal{D} , and we leave the conditioning with respect to \mathcal{D} implicit. For a vector $\bar{a} \in \{0, 1\}^n$, we let $n_1(\bar{a}) = \#\{i : a_i = 1\}$ and similarly for $n_0(\bar{a})$. In particular $n_1(\bar{A}) = n_1$. We'll use the fact that, on an event of probability at least $1 - 4e^{-t}$, it holds

$$\left| n_a - \frac{n}{2} \right| \leq \sqrt{\frac{tn}{2}} \quad \text{for } a \in \{0, 1\}.$$

This is a straightforward application of Hoeffding's inequality. In particular, for $t \leq n/8$, it holds on the same event $\frac{n}{4} \leq n_a \leq \frac{3n}{4}$ for both $a \in \{0, 1\}$.

E.1. Proof of Theorem 5.4

E.1.1. PROOF WITH PERFECT INTERPOLATION

Proof. First, note that thanks to the interpolation assumption,

$$\frac{1}{n_1} \sum_{i:A_i=1} Y_i = 0 = \mathbb{E}[\mathbb{E}[Y_i | A_i = 1, X_i]].$$

We thus need to work only with $\frac{1}{n_0} \sum_{i:A_i=0} Y_i$. We let $a \in \{0, 1\}^n$ with $n_0(\bar{a}) \neq 0$, and define, letting $\bar{X}_{\bar{a}} := \{X_j\}_{\{j: a_j=1\}}$,

$$\mu_{\bar{a}}^{(0)}(\bar{X}_{\bar{a}}) := \mathbb{E}[Y_i | \bar{A} = \bar{a}, \bar{X}_{\bar{a}}],$$

for any i such that $a_i = 0$ (we also integrate wrt the randomness of \mathcal{A} in the expectation). Thanks to Hoeffding's inequality, it holds

$$\mathbb{P} \left(\left| \frac{1}{n_0(\bar{a})} \sum_{i:a_i=0} Y_i - \mu_{\bar{a}}^{(0)}(\bar{X}_{\bar{a}}) \right| > \sqrt{\frac{t}{2n_0(\bar{a})}} \middle| \bar{A} = \bar{a}, \bar{X}_{\bar{a}} \right) \leq 2e^{-t}.$$

Now for two adjacent datasets $\bar{X}_{\bar{a}}$ and $\bar{X}'_{\bar{a}}$, it holds:

$$|\mu_{\bar{a}}^{(0)}(\bar{X}_{\bar{a}}) - \mu_{\bar{a}}^{(0)}(\bar{X}'_{\bar{a}})| = |\mathbb{E}_{\mathcal{A}} \mathbb{E}_{\mathcal{P}_T} [\mathcal{L}(\mathcal{A}(\mathcal{D} \cup \bar{X}_{\bar{a}}), X)] - \mathbb{E}_{\mathcal{A}} \mathbb{E}_{\mathcal{P}_T} [\mathcal{L}(\mathcal{A}(\mathcal{D} \cup \bar{X}'_{\bar{a}}), X)]| \leq \alpha,$$

thanks to the average stability assumption. Thus, using McDiarmid's inequality, it holds

$$\mathbb{P} \left(|\mu_{\bar{a}}^{(0)}(\bar{X}_{\bar{a}}) - \mathbb{E}[Y_i | \bar{A} = \bar{a}]| > \sqrt{\frac{n_1(\bar{a})t\alpha^2}{2}} \middle| \bar{A} = \bar{a} \right) \leq 2e^{-t}.$$

Thus

$$\mathbb{P} \left(|\hat{\tau}_{\text{ATE}} - \mathbb{E}[Y_i | \bar{A} = \bar{a}]| \leq \sqrt{\frac{2t}{n_0(\bar{a})}} + \sqrt{\frac{n_1(\bar{a})t\alpha^2}{2}} \middle| \bar{A} = \bar{a} \right) \geq 1 - 4e^{-t}.$$

We conclude the proof by introducing

$$g(\bar{a}_{-i}) := \mathbb{E}[Y_i | A_i = 0, \bar{A}_{-i} = a_{-i}].$$

The previous bounds allow for a control of $|\hat{\tau}_{\text{ATE}} - g(\bar{A}_{-i})|$. Using again the α -stability, one finds that for two adjacent vectors $\bar{A}_{-i}, \bar{A}'_{-i}$, it holds $|g(\bar{A}_{-i}) - g(\bar{A}'_{-i})| \leq \alpha$. Using McDiarmid's inequality again, we conclude

$$\mathbb{P} \left(|g(\bar{A}_{-i}) - \mathbb{E}[Y_i | A_i = 0]| > \sqrt{\frac{(n-1)t\alpha^2}{2}} \right) \leq 2e^{-t}.$$

Piecing all the inequalities together yields the result. \square

E.1.2. PROOF WITH β -UNIFORM TRAINING STABILITY

Proof. The only difference lies in the way we handle the term

$$\frac{1}{n_1} \sum_{i:A_i=1} Y_i = \frac{1}{n_1} \sum_{i:A_i=1} \mathcal{L}(\mathcal{A}(\mathcal{D}_{\text{train}}), X_i).$$

Like before, we let $\bar{a} \in \{0, 1\}^n$ with $n_1(\bar{a}), n_0(\bar{a}) \neq 0$. We define

$$\mu_{\bar{a}}^{(1)}(\bar{X}_{\bar{a}}) := \frac{1}{n_1(\bar{a})} \sum_{i:a_i=1} \mathcal{L}(\mathcal{A}(\mathcal{D} \cup \bar{X}_{\bar{a}}), X_i)$$

Thanks to β -uniform training stability, it holds that for any adjacent $\bar{X}'_{\bar{a}}$:

$$\begin{aligned} |\mu_{\bar{a}}^{(1)}(\bar{X}_{\bar{a}}) - \mu_{\bar{a}}^{(1)}(\bar{X}'_{\bar{a}})| &\leq \frac{1}{n_1(\bar{a})} \sum_{i:a_i=1} |\mathcal{L}(\mathcal{A}_{\theta}(\mathcal{D} \cup \bar{X}_{\bar{a}}), X_i) - \mathcal{L}(\mathcal{A}_{\theta}(\mathcal{D} \cup \bar{X}'_{\bar{a}}), X_i)| \\ &\leq \frac{1}{n_1(\bar{a})} + \beta. \end{aligned}$$

Using again McDiarmid's inequality, we find that

$$\mathbb{P} \left(\left| \mu_{\bar{a}}^{(1)}(\bar{X}_{\bar{a}}) - \mathbb{E}[Y_i | \bar{A} = \bar{a}] \right| > \left(\frac{1}{n_1(\bar{a})} + \beta \right) \sqrt{\frac{n_1(\bar{a})t}{2}} \middle| \bar{A} = \bar{a} \right) \leq 2e^{-t},$$

where i is such that $a_i = 1$. Like in the previous case, we show that, using this time β -uniform training stability

$$\mathbb{P} \left(\left| \mathbb{E}[Y_i | A_i = 1, \bar{A}_{-i}] - \mathbb{E}[Y_i | A_i = 1] \right| > \sqrt{\frac{(n-1)t\beta^2}{2}} \right) \leq 2e^{-t}.$$

which allows to conclude. \square

E.2. Proof of Theorem B.1

Proof. Using the same reasoning as in the proof with 0-uniform training stability, we can handle the term with $A_i = 0$. For $\bar{a} \in \{0, 1\}^n$, we let $\theta \in \Theta$ be a generic model parameter, and $\hat{\theta}_{\bar{a}}$ be the one obtained after training on $\mathcal{D} \cup \bar{X}_{\bar{a}}$. We define

$$f_{\theta}(X) := \mathcal{L}(\theta, X),$$

so that in particular $Y_i = f_{\hat{\theta}_{\bar{a}}}(X_i)$ on the event $\bar{A} = \bar{a}$. Note that $\hat{\theta}_{\bar{a}}$ is $\bar{X}_{\bar{a}}$ -measurable. Because $\theta \mapsto f_{\theta}(x)$ is L -Lipschitz for all $x \in \mathcal{X}$, the empirical process

$$\theta \mapsto \xi_{\bar{a}}(\theta) := \frac{1}{n_1(\bar{a})} \sum_{a_i=1} f_{\theta}(X_i) - \mathbb{E}_{\mathcal{P}_T}[f_{\theta}(X)]$$

is $2L$ -Lipschitz and centered. Letting $\mathcal{N}_{\varepsilon}$ be a minimal ε -net over $B_{\mathbb{R}^D}(0, B)$, if holds that $|\mathcal{N}_{\varepsilon}| \leq (2B/\varepsilon)^D$, hence

$$\mathbb{P}\left(\sup_{\theta \in \Theta} |\xi_{\bar{a}}(\theta)| > s \mid \bar{A} = \bar{a}\right) \leq 2 \left(\frac{2B}{\varepsilon}\right)^D \exp\left(-\frac{n_1(\bar{a})(s - 2L\varepsilon)^2}{2}\right).$$

Letting

$$s = \sqrt{\frac{2\lambda_t}{n_1(\bar{a})}} + 2L\varepsilon \quad \text{and} \quad \varepsilon = \frac{1}{2L} \sqrt{\frac{2\lambda_t}{n_1(\bar{a})}} \quad \text{with} \quad \lambda_t := t + \frac{1}{2} D \log n_1(\bar{a}) + D \log(4BL),$$

one finds

$$\mathbb{P}\left(\left|\frac{1}{n_1(\bar{a})} \sum_{a_i=1} Y_i - \mathbb{E}_{\mathcal{P}_T}[f_{\hat{\theta}_{\bar{a}}}(X) \mid \bar{X}_{\bar{a}}, \bar{A} = \bar{a}]\right| > 2\sqrt{\frac{2\lambda_t}{n_1(\bar{a})}} \mid \bar{X}_{\bar{a}}, \bar{A} = \bar{a}\right) \leq 2e^{-t}.$$

Now notice that $\mathbb{E}_{\mathcal{P}_T}[f_{\hat{\theta}_{\bar{a}}}(X) \mid \bar{X}_{\bar{a}}, \bar{A} = \bar{a}] = \mu_{\bar{a}}^{(0)}(\bar{X}_{\bar{a}})$. Using a previous bound, we show that

$$\mathbb{P}\left(\left|\frac{1}{n_1(\bar{a})} \sum_{a_i=1} Y_i - \frac{1}{n_0(\bar{a})} \sum_{a_i=0} Y_i\right| > 2\sqrt{\frac{2\lambda_t}{n_1(\bar{a})}} + \sqrt{\frac{t}{2n_0(\bar{a})}} \mid \bar{X}_{\bar{a}}, \bar{A} = \bar{a}\right) \leq 4e^{-t}.$$

For this we conclude easily, since $|\hat{\tau}_{\text{ATE}}|$ is upper-bounded by 1:

$$|\tau_{\text{ATE}}| = |\mathbb{E}[\hat{\tau}_{\text{ATE}}]| \leq \mathbb{E}[|\hat{\tau}_{\text{ATE}}|] \leq \varepsilon + \mathbb{P}(|\hat{\tau}_{\text{ATE}}| > \varepsilon), \quad \text{for all } \varepsilon > 0.$$

□

F. Proofs in the observational setting

Lemma F.1. *Let*

$$\bar{\tau}_{\text{ATE}} := \frac{1}{n_1} \sum_{A_i=1} Y_i - \frac{1}{n_0} \sum_{A_i=0} \frac{\pi(X_i)}{1 - \pi(X_i)} Y_i.$$

It holds, with probability $1 - 2e^{-t}$:

$$|\hat{\tau}_{\text{ATE}} - \bar{\tau}_{\text{ATE}}| \leq \Delta_{\hat{\pi}} + \frac{1}{\eta} \sqrt{\frac{t}{n}}.$$

Proof. We have:

$$\begin{aligned} |\hat{\tau}_{\text{ATE}} - \bar{\tau}_{\text{ATE}}| &= \left| \frac{1}{n_0} \sum_{A_i=0} \left\{ \frac{\hat{\pi}(X_i)}{1 - \hat{\pi}(X_i)} - \frac{\pi(X_i)}{1 - \pi(X_i)} \right\} Y_i \right| \\ &\leq \Delta_{\hat{\pi}} + \underbrace{\frac{1}{n_0} \sum_{A_i=0} \left| \frac{\hat{\pi}(X_i)}{1 - \hat{\pi}(X_i)} - \frac{\pi(X_i)}{1 - \pi(X_i)} \right|}_{:= \xi} - \Delta_{\hat{\pi}}. \end{aligned}$$

Now like in the previous section, we control ξ by conditioning on $\bar{A} = \bar{a}$, applying Höoeffding's inequality for rvs in $[0, C/\eta]$, and finally use the fact that $n_0 \geq n/4$ w.h.p. □

All the proofs in the observational setting mimic the structures of those of the previous section. Thanks to Lemma F.1, one only needs to bound $|\bar{\tau}_{\text{ATE}} - \tau_{\text{ATE}}|$. To ease the notation, we introduce $\zeta(X_i) := \frac{\pi(X_i)}{1-\pi(X_i)}$. As the term involving the Y_i 's for $A_i = 1$ is the same as in the previous section, we only focus on bounding

$$\frac{1}{n_0} \sum_{A_i=0} \zeta(X_i) Y_i - \mathbb{E}[\zeta(X_i) Y_i | A_i = 0].$$

The bound is the same for each settings and the proof goes as follows. We let again $a \in \{0, 1\}^n$ with $n_0(\bar{a}) \neq 0$, and define, letting $\bar{X}_{\bar{a}} := \{X_j\}_{\{j: a_j=1\}}$,

$$\mu_{\bar{a}}^{(0)}(\bar{X}_{\bar{a}}) := \mathbb{E}[\zeta(X_i) Y_i | \bar{A} = \bar{a}, \bar{X}_{\bar{a}}],$$

for any i such that $a_i = 0$. Thanks to Hoeffding's inequality, it holds

$$\mathbb{P}\left(\left|\frac{1}{n_0(\bar{a})} \sum_{i: a_i=0} \zeta(X_i) Y_i - \mu_{\bar{a}}^{(0)}(\bar{X}_{\bar{a}})\right| > \sqrt{\frac{t}{2n_0(\bar{a})\eta^2}} \mid \bar{A} = \bar{a}, \bar{X}_{\bar{a}}\right) \leq 2e^{-t}.$$

Now for two adjacent datasets $\bar{X}_{\bar{a}}$ and $\bar{X}'_{\bar{a}}$, it holds:

$$\begin{aligned} |\mu_{\bar{a}}^{(0)}(\bar{X}_{\bar{a}}) - \mu_{\bar{a}}^{(0)}(\bar{X}'_{\bar{a}})| &= |\mathbb{E}_{\mathcal{A}} \mathbb{E}_{\mathcal{P}_0}[\zeta(X) \mathcal{L}(\mathcal{A}(\mathcal{D} \cup \bar{X}_{\bar{a}}), X)] - \mathbb{E}_{\mathcal{A}} \mathbb{E}_{\mathcal{P}_0}[\zeta(X) \mathcal{L}(\mathcal{A}(\mathcal{D} \cup \bar{X}'_{\bar{a}}), X)]| \\ &= |\mathbb{E}_{\mathcal{A}} \mathbb{E}_{\mathcal{P}_T}[\mathcal{L}(\mathcal{A}(\mathcal{D} \cup \bar{X}_{\bar{a}}), X)] - \mathbb{E}_{\mathcal{A}} \mathbb{E}_{\mathcal{P}_T}[\mathcal{L}(\mathcal{A}(\mathcal{D} \cup \bar{X}'_{\bar{a}}), X)]| \\ &\leq \alpha, \end{aligned}$$

thanks to the average stability assumption. Thus, using McDiarmid's inequality, it holds

$$\mathbb{P}\left(|\mu_{\bar{a}}^{(0)}(\bar{X}_{\bar{a}}) - \mathbb{E}[\zeta(X_i) Y_i | \bar{A} = \bar{a}]| > \sqrt{\frac{n_1(\bar{a})t\alpha^2}{2}} \mid \bar{A} = \bar{a}\right) \leq 2e^{-t}.$$

Thus

$$\mathbb{P}\left(|\bar{\tau}_{\text{ATE}} - \mathbb{E}[\zeta(X_i) Y_i | \bar{A} = \bar{a}]| \leq \sqrt{\frac{2t}{n_0(\bar{a})\eta^2}} + \sqrt{\frac{n_1(\bar{a})t\alpha^2}{2}} \mid \bar{A} = \bar{a}\right) \geq 1 - 4e^{-t}.$$

We conclude the proof by introducing

$$g(\bar{a}_{-i}) := \mathbb{E}[\zeta(X_i) Y_i | A_i = 0, \bar{A}_{-i} = a_{-i}].$$

The previous bounds allow for a control of $|\bar{\tau}_{\text{ATE}} - g(\bar{A}_{-i})|$. Using again the α -stability, one find that for two adjacent vectors $\bar{A}_{-i}, \bar{A}'_{-i}$, it holds $|g(\bar{A}_{-i}) - g(\bar{A}'_{-i})| \leq \alpha$. Using McDiarmid's inequality again, we conclude

$$\mathbb{P}\left(|g(\bar{A}_{-i}) - \mathbb{E}[\zeta(X_i) Y_i | A_i = 0]| > \sqrt{\frac{(n-1)t\alpha^2}{2}}\right) \leq 2e^{-t}.$$

Piecing all the inequalities together yields the result.

G. Additional Experimental Analysis

G.1. Additional details on synthetic data experiment

Data generation process. Training, member and non-member data is generated as follows. Training datapoints $X_i = (a_i, b_i)$ are generated with $a_i \sim \mathcal{N}(0, I_d)$ and $b_i \sim \mathcal{N}(a_i^\top w_\star, 1) | a_i$, for some random fixed unitary vector $w_\star \in \mathbb{R}^d$. This distribution corresponds to \mathcal{P}_T . Non-member datapoints taken from the same distribution (no distribution shift), or taken with $a_i \sim \mathcal{N}(\mu, I_d)$ for some $\mu \in \mathbb{R}^d$, depending on the setting (inducing distribution shift between members and non-members). This shifted distribution corresponds to \mathcal{P}_0 . We consider linear regression with the square loss on such data, and consider the loss-based MIA (that thresholds loss values).

Simulation parameters. Data simulation parameters are as follows:

1. Dimension d , which is not the same in the two training algorithms considered next;
2. Training dataset of size 2000, made of samples from \mathcal{P}_T ;
3. μ is a random unitary vector;
4. w_* is a random standard Gaussian Vector conditioned on having $w_*^\top \mu / \|\mu\| = 0.90$ (correlation between w_* and μ).

Training algorithms \mathcal{A} . We consider the two different algorithms to attack for the MIA:

1. We first consider a setting where our assumptions hold and for which MIAs should have good-to-moderate performances: overparametrized ridge regression, with $\lambda = 10^3$ for regularization parameter, with an ambient dimension $d = 2500$. Definitions 5.2 and 5.3 will hold in this setting due to uniform stability.
2. We then consider a setting for which MIAs should not be able to detect any signal and for which our assumptions hold. We thus consider a gradient-based optimizer that adds Gaussian noise at each step and clips gradient of norm larger than 1, therefore limiting sensitivity of each stochastic gradient batch. We add ℓ^2 regularization with $\lambda = 10$, and $d = 400$ in this setting. The optimizer is DP-SGD, with Gaussian noise $\mathcal{N}(0, 3I_d)$, learning rate of 0.01, 75 epochs and batchsize of 128. This corresponds to DP parameters $(\epsilon, \delta) = (0.602, 0.01)$. Stability will hold in this setting, while interpolation will not (due to DP-SGD noise). β -uniform training stability will hold, as a consequence of uniform stability.

MIA evaluation settings. We consider the three different MIA evaluation settings, corresponding to Algorithms 1 to 3.

1. *Multi Run setting*: 400 training of each algorithm to attack. For each run, the training dataset is made of 2000 samples from \mathcal{P}_T (that stay fixed across all runs), together with another independent sample from \mathcal{P}_T for the first 200 runs (members) and none for the last 200 runs. 200 non-members datapoints are then sampled from \mathcal{P}_T .
2. *1-Run setting*, with only one training run. 2000 samples are drawn from \mathcal{P}_T , forming the training set on which the training algorithm is runned. These 2000 training points are the member dataset. 2000 non-members are then independently sampled from the same distribution \mathcal{P}_T ;
3. *0-Run setting*: training set and members are the same as in the 1-Run setting. The 2000 non-members are here sampled from the shifted distribution \mathcal{P}_0 .

In the multi-run setting there are 200 members and 200 non-members, while in the one-run and zero-run settings there are 2000 of each.

Results. Results for all metrics are reported in Table 2, ROC curves in Figures 3a and 3b. *Raw* metrics mean that they were not adjusted by propensity scores while *Corrected* means that they were (if not specified, correction with true propensity scores, *Learned*: correction with propensity scores estimated via logistic regression). Raw metrics in the 1-Run and 0-Run settings are thus the causal metrics, as well as the corrected ones in the zero-run setting. The raw metrics in the zero-run setting are *not* causal metrics, and our experiments highlight the bias induced by not taking into account distribution shifts. Confidence intervals are made over 100 runs of independent samples from the same data-generating process.

Interpretation. In both settings (DP-SGD, Ridge), Figure 3 shows the ROC curves of the Multi-Run and One-Run settings, that don't have any distribution shift (resp. blue and orange). Then, the ROC curves of the Zero-run setting are shown without correction (green) and with propensity score correction (red). In all these plots, the non-drifted multi-run and one-run ROC curves are essentially the same: interferences are negligible in this case. Due to distribution shift, the zero-run curve shows easier attack surfaces. This is actually a false interpretation since after correction, the corrected zero-run curve matches that of the non-drifted curves. As expected, MIAs are more performant in the Ridge setting than the DP-SGD setting.

In Figure 3b, we plotted the $y = \min(1, e^\varepsilon x + \delta, 1 - e^{-\varepsilon}(1 - \delta - x))$ curve. Under (ε, δ) -DP, a MIA cannot have a ROC curve that crosses that black line in the multi-run setting (Dong et al., 2022). Here, we observe that not adjusting for distribution shift breaks this and yields a ROC curve above this line.

The metrics in Table 2 show the same results through four different causal metrics introduced in Section 3.2. Correction to target the right causal metrics make the zero-run performances match the non-drifted settings. For all metrics and in all settings, the IPW correction makes the causal metrics all align together.

Model	Evaluation	AUC	$\sup_t \tau_{ATE}(t)$	ATE	TPR0.2
Ridge	Multi-run (Raw)	0.561 ± 0.016	0.102 ± 0.023	-287.694 ± 248.990	0.241 ± 0.027
Ridge	One-run (Raw)	0.561 ± 0.019	0.103 ± 0.027	-293.668 ± 189.226	0.243 ± 0.031
Ridge	Zero-run (Raw)	0.669 ± 0.020	0.269 ± 0.031	-1049.710 ± 138.808	0.350 ± 0.041
Ridge	Zero-run (Corrected, Oracle)	0.562 ± 0.026	0.108 ± 0.036	-297.327 ± 151.472	0.201 ± 0.068
Ridge	Zero-run (Corrected, Learned)	0.595 ± 0.025	0.159 ± 0.034	-496.127 ± 106.100	0.228 ± 0.083
DP-SGD	Multi-run (Raw)	0.504 ± 0.018	0.024 ± 0.024	0.633 ± 50.951	0.207 ± 0.024
DP-SGD	One-run (Raw)	0.503 ± 0.017	0.023 ± 0.020	-0.949 ± 46.320	0.205 ± 0.022
DP-SGD	Zero-run (Raw)	0.616 ± 0.016	0.183 ± 0.026	-322.243 ± 41.150	0.299 ± 0.032
DP-SGD	Zero-run (Corrected, Oracle)	0.503 ± 0.024	0.029 ± 0.026	-1.985 ± 68.971	0.165 ± 0.083
DP-SGD	Zero-run (Corrected, Learned)	0.512 ± 0.059	0.063 ± 0.084	-23.022 ± 158.351	0.174 ± 0.111

Table 2. Causal metrics in the three settings (with oracle or learned propensity scores in the zero-run setting), and non-causal metrics in the zero-run setting to highlight the distribution-shift induced bias. $\tau_{ATE}(t)$ is defined as $\tau_{TPR}(t) - \tau_{FPR}(t)$ (Youden's J metric at a given threshold), and $\sup_t \tau_{ATE}(t)$ is thus the largest gap between (causal) TPR and FPR. TPR0.2 is the TPR at FPR $\alpha = 0.2$.

G.2. Additional details on CIFAR10

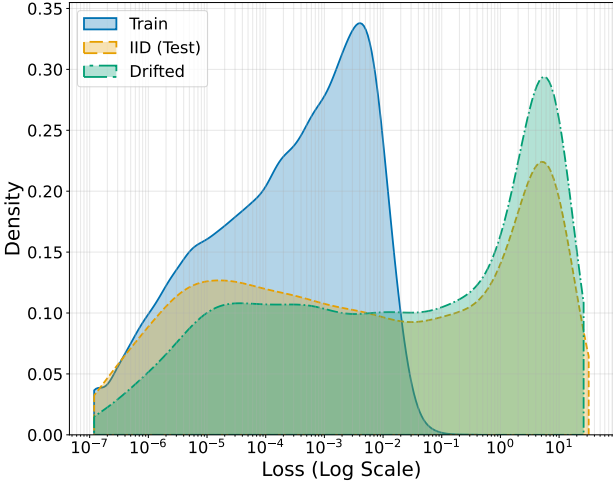
We now present in more details our CIFAR10 experimental setup.

Dataset Construction. We define two base domains: the original clean CIFAR-10 data ($\mathcal{D}_{\text{clean}}$) and a corrupted domain ($\mathcal{D}_{\text{noise}}$) generated by adding Gaussian noise with variance $\sigma = 0.2$ to the images. To ensure valid overlap, we construct the datasets as follows: i) The Members (\mathcal{D}_T) training set is constructed such that 90% of samples are drawn from $\mathcal{D}_{\text{clean}}$ and 10% from $\mathcal{D}_{\text{noise}}$ and ii) The non-members (\mathcal{D}_0) are drawn from a distribution of 10% samples from $\mathcal{D}_{\text{clean}}$ and 90% from $\mathcal{D}_{\text{noise}}$. This design creates a covariate shift: members are predominantly clean, while non-members are predominantly noisy, yet it guarantees that the density ratio remains bounded, since every sample has a non-zero probability of appearing in both sets.

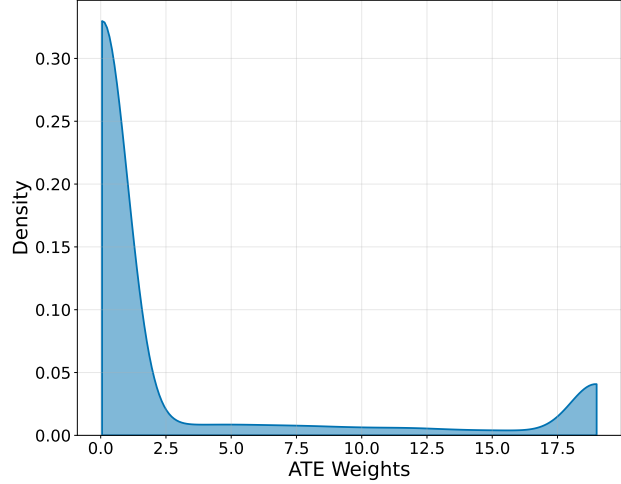
Target Model. On this dataset, we train a ResNet-16 (He et al., 2016) architecture trained on. The model is optimized using Stochastic Gradient Descent (SGD) with a batch size of 128 and a fixed learning rate of 0.01. Training is performed for 10000 optimization steps. To isolate the effects of distribution shift and memorization without additional confounders, we train the model without any data augmentation.

Propensity Score Estimation. To correct for this distribution shift, we estimate the propensity score $\pi(x) = \mathbb{P}(A = 1 | X = x)$. We treat this as a binary classification problem, distinguishing between the member distribution \mathcal{D}_T and the non-member distribution \mathcal{D}_0 . We fine-tune a ResNet model (He et al., 2016) pre-trained on ImageNet (Deng et al., 2009) to minimize the binary cross-entropy loss. We perform this estimation using cross-validation: the propensity model is fitted on a held-out portion of the data mixtures, ensuring that the estimated weights $\hat{\pi}(X_i)$ are independent of the MIA scores Y_i used for the final evaluation.

Results. We compare the performance of Membership Inference Attacks across the three evaluation regimes. Figure 3c displays the ROC curves for the loss-based attack. The *IID (Test)* curve (blue) represents the idealized setting where \mathcal{D}_0 follows the same distribution as the training set (\mathcal{D}_T). The *Drifted* curve (orange) shows the naive zero-run evaluation where non-members are drawn from the shifted (noisy) distribution. This induces an inflation in attack performance ($AUC \approx 0.75$), misleadingly suggesting high memorization. However, this advantage is spurious: it stems from the model's high loss on noisy non-members rather than true privacy leakage. By applying our propensity score correction (green curve), we recover the true causal memorization signal ($AUC \approx 0.66$), which aligns closely with the valid IID baseline ($AUC \approx 0.65$). This confirms that our method successfully removes the bias.



(a) Loss Distributions



(b) Propensity Weights

Figure 4. Additional metrics. (a) The loss distribution for drifted non-members is shifted, making them more distinguishable from members without true memorization. (b) The distribution of estimated ATE weights shows how our method corrects this by upweighting the minority of non-members that are distributionally similar to the training set.

To better understand the source of bias in the zero-run setting, we analyze the distributions of losses and the estimated propensity weights for the CIFAR10 case. Figure 4a visualizes the density of loss values for training members (Train), IID test non-members, and Drifted non-members. The *Drifted* distribution (orange) is shifted significantly to the right (higher loss) compared to the *IID* distribution (blue). Because standard MIAs predict membership based on low loss, the separation between the low-loss members and high-loss drifted non-members is artificially large, leading to the inflated AUC observed in the main text. The overlap between the Train and IID Test distributions is bigger, reflecting the attack’s true performance.

Propensity Weights. Figure 4b shows the distribution of the inverse probability weights (IPW) applied to the non-member samples during our correction. The distribution is heavy-tailed, assigning high weights to the rare non-members that resemble the training distribution (low noise) and low weights to the abundant noisy samples.